Universidade de Lisboa
Faculdade de Ciências
Departamento de Física

Clinical Implementation of 3D EPID *In Vivo* Dosimetry for the Elekta LINAC

Sara Lopes Silveira

Mestrado Integrado em Engenharia Biomédica e Biofísica
Perfil em Radiações em Diagnóstico e Terapia

Dissertação orientada por:

Dr. Joep Stroom, Departamento Radioterapia, Fundação Champalimaud

Prof. Dr. Luís Peralta, Faculdade de Ciências da Universidade de Lisboa

2015

Resumo

A radioterapia tem vindo a ocupar um lugar de elevada importância no que concerne a tratamentos do foro oncológico. Tendo como base a radiação ionizante, tem por objetivo destruir ou eliminar a ação proliferativa das células cancerígenas, salvaguardando ao máximo os tecidos saudáveis. Novas técnicas de radioterapia têm surgido no sentido de tornar o tratamento mais eficaz: a implementação da Radioterapia de Intensidade Modulada (IMRT), Terapia de Arco Volumétrico (VMAT), bem como a introdução de tratamentos hipofracionados. O crescente aumento da complexidade dos campos, aumentou a necessidade da obtenção de uma elevada precisão das atuais práticas de verificação da dose. Neste sentido, têm sido introduzidos procedimentos de Controlo Qualidade (QA) com o intuito de verificar o grau de precisão com que o acelerador linear (LINAC) entrega a dose planeada. Estes procedimentos podem ser realizados antes (pré-tratamento) ou durante (*in vivo*) o tratamento. É importante referir que são duas práticas complementares, sendo que o pré-tratamento é capaz de detetar um erro antes da primeira fração de tratamento enquanto na dosimetria *in vivo*, é possível detetar todos os erros que ocorram durante o mesmo. Erros esses, derivados da respiração e movimentação do paciente, bem como possíveis alterações anatómicas que possam ocorrer ao longo das frações.

O pré-tratamento é o procedimento mais frequente na maior parte dos centros de radioterapia. Na Fundaçao Champalimaud, o QA consiste na irradiação do plano clínico num fantoma constituído por díodos (ArcCHECK). Posteriormente é feita a análise da distribuição de dose obtida e a sua comparação com o planeado. Relativamente à dosimetria *in vivo*, começou inicialmente por ser realizada com dosímetros, como os díodos. No entanto, para além de necessária a sua colocação na pele do paciente, estes detetores apenas indicam a dose num conjunto finito de pontos. Perante as desvantagens apresentadas, tem vindo a ser estudado a utilização dos dispositivos de imagem portal (EPID), uma vez que as imagens adquiridas contêm informação sobre a dose. O EPID encontra-se acoplado ao LINAC (lado oposto à gantry) acompanhando o seu movimento, durante a irradiação. No início do século, começou a ser desenvolvido um algoritmo de retroprojeção com o intuito de relacionar a dose ao nível do EPID com a dose dentro do paciente/fantoma. Neste sentido, a dose é

reconstruída dentro do paciente em múltiplos planos paralelos ao EPID, para cada ângulo da gantry.

O presente projeto teve como principal objetivo, a implementação clínica dosimetria *in vivo*, com recurso ao EPID e estudar quais os fatores que influenciam os seus resultados. Para tal, foi testado um software de dosimetria *in vivo* com EPID (PDapp), desenvolvido pelo Instituto do Cancro Holandês – Antoni van Leewenhoek (NKI-AVL). Desta forma, foram irradiados 193 pacientes com cancro da mama pela técnica IMRT e medidos com EPID. Posteriormente a dose medida foi calculada e comparada com a dose planeada pelo PDapp. A comparação das doses foi efetuada através do método de avaliação gama, cujos critérios foram 3% de diferença de dose e 3 mm de distância de concordância (DTA). Foi, em média, obtida uma sub-dosagem sistemática onde as doses deferiram entre si em -1,5%. Foi obtido também um γ_{mean} de 0.61 e $\%\gamma < 1$ de 83%. Estes resultados são promissores, uma vez que têm em conta o movimento do paciente durante o tratamento, bem como as suas alterações anatómicas. Observou-se também que tanto o output, como os interlocks do LINAC influenciavam os resultados do EPID. Contudo, a nossa proposta inicial seria substituir o atual procedimento de pré-tratamento pela dosimetria *in vivo* com recurso ao EPID, uma vez que um erro ocorrido na primeira fração poderia ser corrigido nas frações seguintes (15 frações – cancro da mama). Contudo, o departamento de radioterapia não quis abandonar o pré-tratamento e neste sentido foi desenvolvido um software de pré-tratamento com EPID a partir dos dados fornecidos pelo PDapp. A ideia passa por verificar a dose que irá ser entregue ao paciente através de open fields (irradiação do plano do paciente sem nenhum meio de atenuação, como o fantoma, e consequente aquisição de imagens com EPID). Um grupo de 10 pacientes de mama IMRT e 9 VMAT foram medidos e avaliados. Em termos médios foi obtido um γ_{mean} de 0.47 e 0.57 respetivamente.

Após realização deste projeto foi possível concluir que a dosimetria com EPID é uma ferramenta precisa e rápida para verificação da dose *in vivo* em pacientes com cancro da mama tratados com a técnica IMRT. Por outro lado, o pré-tratamento realizado com EPID demonstrou ser mais preciso e menos demorado do que a atual prática com o fantoma ArcCHECK. Embora o pré-tratamento com EPID seja um método em desenvolvimento, foram obtidos resultados bastante encorajadores ao ponto de continuar o seu desenvolvimento para que seja possível a sua futura implementação.

Palavras-chave: Controlo Qualidade; Dosimetria *In vivo*; Pré-tratamento; Dosimetria com EPID; Cancro da mama.

Abstract

Radiotherapy is immensely important in the treatment of cancer patients. As the complexity of radiotherapy increases, with the implementation of Intensity-Modulated Radiation Therapy (IMRT) technique and the introduction of hypofractionated treatments, so does the need for high accuracy in dosimetric verification. In response to this need, Quality Assurance (QA) procedures have been introduced to verify the dose before (pre-treatment) and during (*in vivo*) the treatment. These are two complementary procedures insofar as pre-treatment dosimetry is able to detect an error before the first fraction is given and *in vivo* dosimetry can detect any errors that occur during the treatment (e.g., patient's position and or anatomical changes).

The pre-treatment QA is the most common procedure followed in most radiotherapy centres. At Champalimaud Foundation the QA is performed by irradiating the clinical plan on a cylindrical detector array (ArcCHECK). Afterwards an analysis is made of the obtained dose distribution and the planned dose. *In vivo* dosimetry was first implemented through the use of dosimeters, such as diodes, but because the detectors are located on the patient's skin they measure the dose only at those finite points. In view of the disadvantages presented, the Electronic Portal Imaging Devices (EPID) has been studied. These were initially used for set-up patient verification and then, as a tool of dose verification. These devices are able to acquire portal images of the treatment beams and it is possible to correlate the pixel intensity to dose information. At the beginning of this century, a back-projection algorithm was developed in order to correlate the dose at the EPID level to the one inside the patient/phantom. In this way, the dose is reconstructed within the patient volume in multiple planes parallel to the EPID for each gantry angle.

The main goal of this project was to examine the clinical implementation of the EPID *in vivo* dosimetry and to study the factors that will influence these results. An EPID *in vivo* dosimetry software, called PDapp, developed by Nederlands Cancer Institute Antoni van Leewenhoek (NKI-AVL) was tested. We measured 193 IMRT breast patients and then evaluated with PDapp. A gamma evaluation method was used with a dose-difference criterion of 3% and distance-to-agreement (DTA) of

3mm. On average, a systemic under-dose was obtained in which the planned and measured dose differ by -1.5%. A γ_{mean} of 0.61 and $\%\gamma < 1$ of 83% were acquired. These results are promising since they account for patient's movement during the treatment as well as anatomic changes. It was also noticed that the LINAC output and interlocks influence the EPID results. Our initial proposal was to replace the current pre-treatment by EPID *in vivo* dosimetry, since an error occurring in the first fraction could be corrected in the following fractions. However, the radiotherapy department wished not to abandon pre-treatment, so we developed an EPID pre-treatment software from the existing PDapp method. The idea was to check the dose that is going to be delivered to the patient through the open fields only. A group of 10 IMRT and 9 VMAT breast plans showed that the patient-averaged γ_{mean} of 0.47 and 0.57 respectively ($\gamma = 1$ means a dose of 3% or 3mm error).

We concluded that the EPID dosimetry method is an accurate and fast tool for *in vivo* dose verification of IMRT breast plans in 3D. On the other hand, EPID pre-treatment QA proved to be more accurate and is less time consuming than the current practice with the ArcCHECK. Although EPID pre-treatment QA is a method under development, encouraging results were obtained that suggest it is valuable to continue developing its application.

Key-words: Quality Assurance; *In vivo* dosimetry; Pre-treatment; EPID dosimetry; Breast Cancer.

Acknowledgments

"*Those who pass us by, do not go alone, do not leave us alone. Leave a little piece of yourself, take a little of us*"

Antoine de Saint-Exupery

First of all, I am very thankful to Champalimaud Foundation for receiving me at Radiotherapy department. I would like to express my gratitude to Joep and Sandra for giving me the opportunity to do this internship. My supervisor, Joep Stroom specially thanks for your guidance, patience, encouragement and for everything I learned with you. It was also privilege to deal with Sandra Vieira for her sympathy, concern and helpfulness. It was a pleasure to spend this year at Radiotherapy department, surrounded by amazing and expert people, especially Daniela for being so friendly and always with a smile on her face.

Gostava também de agradecer ao Professor Luís Peralta, o meu orientador interno, por todo o apoio dado e preocupação demonstrada ao longo deste árduo percurso.

A todos os meus amigos, um grande obrigado por terem estado sempre do meu lado. Um especial agradecimento à Tatiana Ladeira por ter feito esta caminhada comigo, por todos os bons momentos e por toda ajuda dada. A ti, Sara Ferreira por teres tido um papel fundamental ao longo destes 5 anos de curso. E à Ritinha por me apoiar incondicionalmente, por estar sempre presente nos momentos mais difíceis e por celebrarmos sempre juntas as nossas conquistas!

Por último e mais importante, gostaria de agradecer à minha Família. Em especial aos meus Pais, Irmão e Tia pela presença em todos os momentos, por me fazerem acreditar que sou capaz. Obrigada Mãe, por estares sempre presente, chorares e por rires comigo, por largares tudo para me ajudares, por todo o amor e carinho. Tenho um enorme orgulho em ti! Obrigada Pai por todas as horas de lazer e diversão que proporcionaste ao longo deste caminho bem como todas as palavras de incentivo na hora certa. Obrigada pelo teu ombro amigo, sempre disponível para me ajudar. A ti

Jorge, por fazeres parte da minha família e amigos, pela força transmitida, paciência e companheirismo. Nada disto teria sido possível sem vocês!

Não poderia deixar de mencionar a minha grande fonte de inspiração ao longo destes 5 anos, a minha Bisavó Margarida. Foste e serás sempre a minha força pela grande Mulher que foste e apesar de não estares presente, sei que estás orgulhosa de mim.

Contents

List of Tables

List of Figures

List of Abbreviations

IMRT	Intensity-Modulated Radiation Therapy
VMAT	Volumetric Modulated Arc Therapy
QA	Quality assurance
EPID	Electronic Portal Imaging Device
LINAC	Linear Particle Accelerator
DNA	Deoxyribonucleic acid
MeV	Megaelectron Volt
MLC	Multi Leaf Collimator
Gy	Gray
3D-CRT	3D Conformal Therapy
CT	Computed Tomography
OAR	Organs at risk
PTV	Planning target volume
SIB	Simultaneous-integrated boost
LQ	Linear-quadratic model
TPS	Treatment Planning System
DVH	Dose-volume histogram
MU	Monitor unit
CP	Control Point
MCS	Modulation complexity score
SAS	Small aperture score
MFA	Mean field area
A-si EPID	Amorphous silicon EPID
NKI-AVL	Nederlands Cancer Institute Antoni van Leewenhoek
FET	Field-effect transistor
IC	Ionization chamber
MV	Megavolt
DICOM	Digital Imaging and Communication in Medicine
DRR	Digitally Reconstructed Radiograph
DTA	Distance-to-agreement

Chapter 1

Introduction

Cancer is one of the leading causes of death worldwide, with approximately 14 million new cases and 8.2 million cancer related deaths in 2012. It is expected that the number of new cases will rise 70% over the next two decades [2]. "Breast cancer is the top cancer in women worldwide and is increasing particularly in developing countries where the majority of cases are diagnosed in late stages." [3].

These statistics are mainly associated with developed countries with poor diet (30%), tobacco (16%), and sedentary life [4]. Most of the tumours that at the time of initial diagnosis have not spread to distant locations can potentially be cured by interventions like surgery, radiotherapy, chemotherapy or combinations of these. After conservative breast surgery, radiotherapy has an integral role in treating breast cancer. Radiotherapy uses ionizing radiation to kill or damage cancer cells and stop them from growing and multiplying. As those cells are very sensitive to treatment fractionation, i.e., reduction in the number of fractions and subsequent dose escalation. This increment provides a more effective treatment without increasing the toxicity to healthy tissues.

Technological developments allowed not only higher complexity techniques, such as IMRT and VMAT, but also higher prescribed doses. Therefore, the need to develop new dose verification techniques has emerged in order to prevent accidents during the treatment. In November of 2000, at the National Institute of Panama, 28 patients were irradiated with high overdoses due to a software error. This error led to the death of 17 of the 28 patients, three years later [5]. According to the International Atomic Energy Agency in Epinal, France, between May 2004 and May 2005, 23 patients with prostate cancer received an exposure that exceeded between 7% and 34% of the prescribed dose. Among the patients involved in the accident, four died and 19 developed serious late complications, including rectal inflammation

[6].

As a result, daily QA is currently performed by pre-treatment verification, which checks if the LINAC (Linear Particle Accelerator) can deliver the dose according to what is intended. This procedure is performed with the aim of detecting possible errors before treatment is given to the patient. It should be noted that although the error detection before treatment is important, there are errors that can occur only during treatment. Hence, *in vivo* dosimetry has emerged which consists of determining the dose distribution to the patient during the treatment. The first studies of *in vivo* dose verification were performed by placing diodes on the patient's skin to obtain the dose at specific points. In order to obtain the dose throughout the plan, research is addressing the use of EPID to do the pre-treatment and the *in vivo* dose verification instead of patient set-up verification. The EPID is a device attached to the LINAC located at the opposite side to LINAC's head following its movement. It measures the intensity of the radiation transmitted by the patient/phantom during irradiation by acquiring portal images.

The above mentioned incidents have alerted national safety authorities and, as a consequence, several countries are currently developing regulations that make *in vivo* dosimetric verification mandatory. This project seeks to develop the clinical implementation of EPID *in vivo* dosimetry for ELEKTA LINAC, for breast cancer patients, in particular.

Chapter 2

Background

2.1 Breast Cancer Radiotherapy

In the initial stage of a breast tumour, usually a conservative breast surgery is performed in which only the tumour volume is removed (lumpectomy), followed by whole breast radiotherapy. This procedure is considered to be as effective as mastectomy, in which the entire breast is removed. Several studies have been performed in an attempt to improve the effectiveness of the treatment, mainly the introduction of an extra irradiation (boost) in the region where the tumour was removed. However, it is still unclear what the best way is to incorporate the boost irradiation in order to obtain the best results from a radiobiological perspective [7].

2.1.1 Normal and Hypofractionated Treatments

Traditionally, radiotherapy following conservative breast surgery requires about seven weeks of daily treatment. Two Gy per fraction during five weeks (25 fractions) are delivered which makes a total of 50 Gy. The total breast irradiation is carried out separately from an additional irradiation of the regions where the tumour was removed (boost region), consisting of 3-8 boost fractions for one or two weeks.

In recent decades a need to irradiate the total breast and the boost region simultaneously has become increasingly evident. The implementation of SIB (Simultaneous-integrated boost) technique is now possible thanks to the development of IMRT and new imaging techniques that allow precisely locating the position of the patient immediately before treatment [8].

One of the principles of radiobiology states that the long-term effects on normal

tissues are strongly dependent on the amount of dose per fraction. According to the linear-quadratic (LQ) model, the sensitivity of the tissues to fractionation is quantified by the ratio α/β and the higher the sensitivity of tissues to an increase of dose per fraction, the lower the ratio [9].

To be able to integrate the total breast irradiation with the boost region, it is necessary to analyse healthy tissue implications to an increase of dose. Therefore, the higher the dose per fraction, the greater the susceptibility of healthy tissues to radiation. The LQ formulation enables to model the biological response to the radiation in both healthy and tumour cells. This model assumes that there are two mechanisms to cell death by radiation: single ionizing events that causes the breakage of the double DNA strand (type α) and two separate ionizing events (type β) – Figure. Type β events breaks a single DNA strand, therefore if the damage resulting from the first event is repaired before the second event occurs, it is not lethal for the cell [10].

$$SF = exp(-\alpha D - \beta D^2) \tag{2.1}$$

Where D is the dose in Gy. In biological terms the α/β is the radiation dose at which the linear and quadratic contributions to cell kill are equal, since type α predominates at doses of magnitude less than α/β, while, type β predominates at higher doses. [11].

The surviving fraction of cells that retain their reproductive integrity, under specific treatment conditions, is described in Figure 2.1.

Breast cancer cells are more sensitive than most other tumours to the effects of fraction size with a low α/β of 4 Gy. By contrast, epithelial cancer has α/β of 10 Gy which is considered insensitive to a fraction dose increase. Therefore, in breast cancers, fewer larger fractions (hypofractionation) can be more efficient than the conventional fractionated treatment, without necessarily increasing the toxicity. However, in order to protect and avoid excess late normal tissue toxicity, the overall total dose must be reduced [13].

At the Champalimaud Foundation (Portugal), breast cancer treatments are undertaken with the IMRT sliding window technique or VMAT and 15 hypofractionated fractions of 2.7 Gy each (3 treatment weeks). In boost cases, a SIB technique is used which usually results in deposition of 3.2 Gy in the boost region per treatment

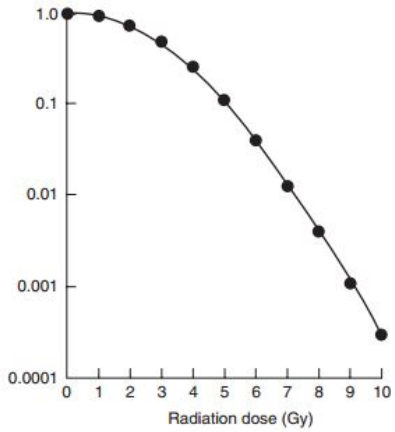

Figure 2.1: Cell survival curve as a function of absorbed radiation dose [12].

fraction. The advantages of this technique compared to conventional radiotherapy with a sequential boost (widely used) are: reduction of treatment time by reducing the number of fractions; better dose distribution through reducing the dose in OARs (Organs at Risk); better dosimetric coverage in boost zone; reduced time available for tumour growth during the treatment; low levels of toxicity (such as fibrosis and oedemas) especially in deeper tumours, and a better preservation of the skin [14].

2.2 Radiotherapy

Radiotherapy is an oncological treatment that seeks to destroy cancer cells while minimizing the risk to healthy tissues. The phase of the cell cycle is important in cancer therapy since the cells that are in division phase (mitosis) or in G2 phase (preparing to divide) are more sensitive to ionizing radiation. This sensitivity is related to the high level of DNA compression, which results in a greater probability of radiation damage. There are two mechanisms for cell death by radiation: single ionizing events that cause the double DNA strand to break, and two separate ionizing events. Tumor cells have the particularity of dividing rapidly and uncontrollably and are therefore more susceptible to the damaging effects of radiation as compared to healthy cells [15].

2.2.1 Physics of Radiation Therapy

External radiotherapy is based on interactions of ionizing radiation with matter in order to kill or eliminate the reproductive capacity of malignant cells. To accomplish this, a LINAC is used to produce high energy photons that can be directed with a high level of accuracy and precision.

2.2.1.1 Production of High Energy Photons

Electrons are first produced in an electron gun by thermoionic emission and injected into the waveguide of the LINAC. The heated cathode emits electrons into a vacuum where they are accelerated across an initial kilovoltage. Using radiofrequency waves, the electrons are accelerated to the desired MeV kinetic energy. Magnets in the beam transport system conduct the electrons from the waveguide to the treatment head. Then, the high energy electrons bombard a metal target with a high atomic number and, due to the Bremsstrahlung effect, photons are produced and emitted [16].

2.2.1.2 Collimation System

The high energy photons generated are first collimated by a primary collimator, and then pass through a filter (flattening filter), which makes the photon beam more homogeneous (uniform). After that, the flattened x-ray beam crosses a system of ionization chambers where the dose rate is monitored (Figure 2.2) [17].

To ensure that the shape of the delivered x-ray beam matches the shape of the tumour, a final collimation system is used. This is done using a MLC (Multi-Leaf Collimator), which is composed of 40 leaf-pairs of absorbent tungsten located at opposite sides which move independently of each other and can create a variety of complex beam shapes. An upper (Y) and lower (X) jaws (secondary collimator) are positioned above and below the leaf-pairs respectively. The maximum aperture of each leaf-pair is 40 cm, but the transmission factor as the maximum travel speed are specific characteristics of each type of MLC. The Y jaws track the MLC movement in a horizontal direction in order to decrease the interleaf radiation transmission. As a consequence, they define the field width, while the X jaws moves perpendicularly to the direction of MLC leaf, defining the field height [18].

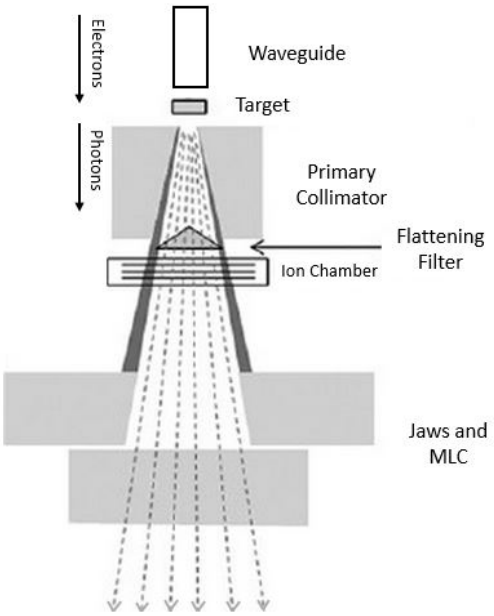

Figure 2.2: Schematic configuration of LINAC. Adapted from [1].

2.2.2 Depth Dose

First, it is important to define the SI unit responsible for describing the amount of energy deposited in tissues. This quantity is denoted by Gray (Gy), and is equivalent to 1 Joule per kilogram (1 Gy = 1 J/Kg). Therefore, the absorbed dose is given by the quotient of the average energy transmitted by ionizing radiation ($d\overline{E}$) and the corresponding mass (dm):

$$\mathrm{D} = \frac{d\overline{E}}{dm} \tag{2.2}$$

The basic principle inherent to external radiotherapy is the use of an ionization source that is located at a certain distance from the patient. At the Champalimaud Foundation a source of photon beams is used, but electron or proton beams could also be used. It is essential to understand the way the radiation is absorbed by the patient.

The megavoltage photon beam propagates through air or vacuum according to the inverse square law, which expresses the relationship between the energy per unit area and distance. According to this law, the intensity (I) at a specific point is inversely proportional to the square of the distance from the source (d) and is given

by:

$$I \propto \left(\frac{1}{d}\right)^2 \tag{2.3}$$

In a patient or a phantom (device used to simulating the effect of radiation on tissues), besides the inverse square law, there are other factors, such as the attenuation and photon scattering which are responsible for the curve's shape of the dose deposition along the depth (Figure 2.3).

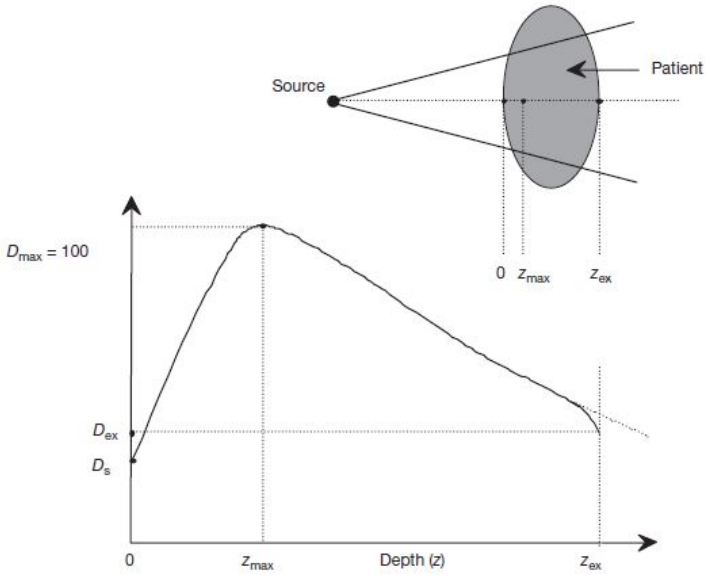

Figure 2.3: Deposited dose in a patient. D_s is the dose received by the patient surface. At z_{max} depth, the dose reaches its maximum value and D_{ex} is the dose at the exit patient point [16].

The photon beam enters at the patient surface and delivers an amount of dose D_s. As the beam penetrates the deposited dose increases until a certain depth z_{max}. From that depth the dose decreases almost exponentially until it reaches a value D_{ex} at the patient exit point. The maximum absorbed dose depends mainly on beam energy and absorbent material, but also on the field size [16].

2.2.3 Delivery Techniques

The introduction of 3D-CRT (3D Conformal Therapy) came up with the appearance of planimetry systems. This fact allows not only a faster but also a more accurate dose distribution calculation. The technique is based on patient CT (Computed Tomography) and it provides a conformation of the beams according to the target volume and OARs. This technique is limited by the geometrical conformation of the beam. In case of having irregular PTV (Planning Target Volume), 3D-CRT is not capable of separating the dose in the target volume from the healthy tissues [19].

As a consequence of 3D-CRT limitation and with the arrival of MLC, the IMRT technique was introduced in the 1990s. The MLC is controlled automatically by computer, and allows for achieving the desired conformation/field geometry. In addition to the modulation of beam conformation, the MLC also allowed the modulation of the beam intensity. This feature allows for minimizing the dose to healthy tissue and optimizing the dose distribution in the target volume.

The IMRT technique is divided into IMRT with fixed angle or rotational (VMAT). In the first case, the modulation of beam intensity is achieved using the MLC in static mode (step and shoot) or in dynamic mode (sliding window). In the case of step and shoot, the intensity modulation is obtained by subdividing the beam in several segments (subfields) in which each has a uniform intensity. It is important to note that the irradiation occurs only when the MLC leaves are stationary, which means that they have already achievd the desired conformation. In the sliding window mode, used at Champalimaud Foundation, the beam intensity is modulated through MLC movement during the irradiation. It is the variation of the position and speed of the leaves that allows the creation of a modulated intensity profile [20].

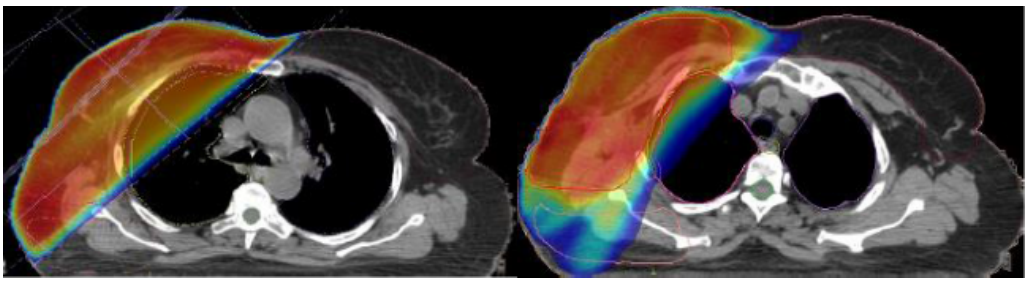

Figure 2.4: Breast plans comparison between 3D-CRT (left) and IMRT (right) techniques for the same patient [21].

Analysing two dose distributions from the different techniques (Figure 2.4), one sees that both plans have beam conformation, since the OAR irradiations are

avoided. However, for the IMRT technique there is also the beam intensity modulation, which leads to a higher dose at the target volume and the healthy tissues with significantly reduced dosages. The same does not occur with 3D-CRT, as all the irradiated volume has the same dose [21].

The VMAT technique was introduced in 2007 and uses the MLC in dynamic mode, while the gantry rotates around the patient and delivers the dose distribution simultaneously. In this way, the MLC adjusts to the target volume shape at each moment, as the gantry is making a complete or a partial arc. The main benefit is speed.

2.2.4 Radiotherapy Chain

Each clinical process is complex, and involves several steps in order to guarantee that the treatment is given in the best possible way (Figure 2.5).

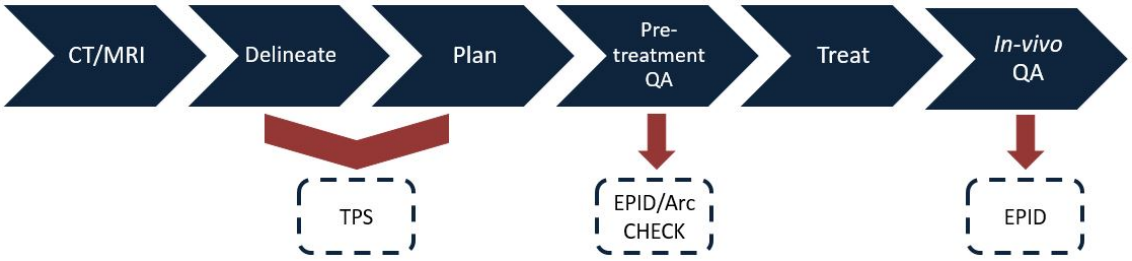

Figure 2.5: Radiotherapy chain.

First of all, the radiation oncologist evaluates the disease stage and decides between a curative or palliative treatment. Depending on the tumour type, it is decided which treatment or combined treatments will be used, i.e., radiotherapy, chemotherapy or surgery. For radiotherapy, the procedure starts with a patient anatomical image using a CT or Magnetic Ressonance Imaging (MRI). The radiation oncologist then delineates the target volume as OARs from the CT acquired, and also defines the dose prescription. With the relevant volumes delineated, the next step in the treatment plan process is to calculate the dose and optimize the dose distribution obtained. This step is performed by dosimetrists with the support of TPS (Treatment Planning Systems), which will be explained in the next subchapter. The dose distribution is then evaluated by a physicist who checks the dose constraints for normal tissue and target volume. One approach would be to use cumulative dose-volume histograms (DVH). A DVH is an important and powerful tool for quantitative evaluation of treatment plans that summarizes the information contained in 3D dose distributions. Consequently, it can be checked if the target volume is correctly covered by the prescribed dose and if the OARs irradiation does

not exceed the tolerances recommended internationally. The final approval of the treatment plan is done by the radiation oncologist, who decides whether the plan meets the objectives and restrictions defined, or if a new plan calculation is required [22],[23].

2.2.5 TPS

The TPS is a computer software that receives patient information to generate beam shapes and dose distributions according to the dose constraints that each tissue could have. It is also capable of making plan evaluations through DVHs and transfering the plan to the treatment machine. Dose calculations have evolved from 2D models to 3D models and from there to 3D Monte-Carlo simulations.

The patient information is then stored in a medical imaging standard format, namely DICOM (Digital Imaging and Communication in Medicine). DICOM-RT is specific for radiotherapy and incorporates different types of information such as: RT Structure, which contains the delineation of the relevant structures; RT Plan, with all the dosimetric and geometric information of the treatment plan; RT dose, with the dose distributions calculated by the TPS [24].

It is important to mention that the RTP is a file format also used in radiotherapy for exporting and importing information about treatment planning data. This file may not contain as much information as the DICOM-RT Plan, but it is used by the LINAC to deliver the treatment.

According to the type of technique, the TPS uses two different approaches to perform the dose calculation. The 3D-CRT technique uses forward treatment planning that requires a previous choice of specific parameters such as beam selection, energies, and MLC configuration, before dose calculation. With the implementation of the IMRT technique and as computers became faster, an automated treatment planning algorithm was introduced. Unlike forward treatment planning, in so called "inverse" treatment planning the first step is to introduce a predefined number of dose restrictions corresponding to each type of tissue and the prescription dose. The software then automatically calculates the optimal beam modulation in order to meet the chosen thresholds [23].

The Monaco software is the TPS from Elekta which uses a Monte Carlo algorithm, the most accurate dose calculation available. This system uses biological cost functions that allow to model tissue dose responses. It uses a multi-criteria optimization that automatically seeks to achieve better normal tissue sparing without

compromising PTV coverage. In relation to IMRT plans, the dose deposition is made from several oblique radiation fields, called anterior right and left and oblique posterior right and left (OAD, OAE, OPD, and OPE respectively) according to the direction of the beam. After performing dose calculation, Monaco is capable of creating cumulative DVHs for healthy tissue and tumour volumes. Monaco is connected to Elekta's MOSAIQ, which is a patient oncology information management system. MOSAIQ connects the TPS with the treatment machine by allowing the transference of patient information such as the treatment plan.

2.3 QA

The implementation of IMRT and VMAT techniques increases the demand for more effective methods to measure the accuracy with which the planned dose is delivered to the patient. Besides the daily verification of every component used (e.g. the output verification), the pre-treatment verification of each patient is also included. The physicists perform a plan verification that involves checking the LINAC deliver accuracy of the planned treatment. This step evaluates a simulation of the plan; MU delivered, and the correct transfer of the plan to the treatment machine. Since the pre-treatment is accomplished immediately before the patient treatment, one can question the importance of measuring the dose being deposited in the patient during treatment (*in vivo* dosimetry). This need emerges due to the accidents mentioned earlier, e.g. the Panama case, which could be detected only with *in vivo* dosimetry [25].

2.3.0.1 Pre-treatment

For pre-treatment QA, the patient plan is calculated in a phantom with detectors that measure the dose received. The measured dose is then compared to the respective dose calculated by the TPS.

The Champalimaud Foundation uses the ArcCHECK, which is a cylindrical PMMA (polymethyl methacrylate) phantom that is composed of a 3-dimensional matrix with 1386 diodes, arranged helically (Figure 2.6).

These pre-treatment QAs are made the day before the first treatment fraction. It is also possible to perform the pre-treatment QA with EPID (Figure 2.7) instead of the ArcCHECK, but this it is not yet implemented clinically, although it is included herein. This replacement would be advantageous since the EPID has a more rapid acquisition of images with a greater accuracy (mm), while the ArcCHECK has a

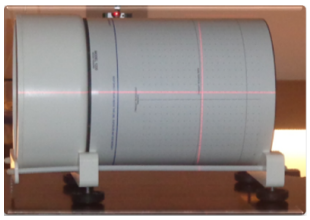

Figure 2.6: ArcCHECK phantom.

precision in cm. The portal images present a better resolution and thus yield the most accurate dose verifications.

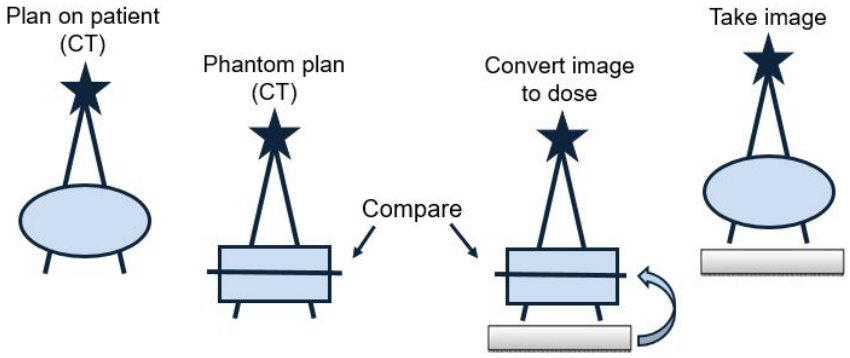

Figure 2.7: Schematic presentation of pre-treatment QA procedure.

Pre-treatment detects errors such as incorrect positioning of the MLC leaves; incorrect plan export from the TPS to the LINAC; or any accidental changes occurring in the plan [26].

However, during pre-treatment QA, there are some plans whose measured and planned doses differ beyond acceptable variation. A rejected plan needs to be recalculated and measured again before it is approved for clinical use. For that reason it is extremely useful to find a relationship between the treatment parameters and the QA results. Using a metric that is strongly correlated with treatment plan would help to avoid the parameters that are related to a bad QA result. This procedure will decrease the time required for pre-treatment QA.

2.3.0.1.1 State of the Art A study was published in 2010, that enables the comparison between the number of MU and a new metric called MCS (Modulation Complexity Score) with quality assurance processes. A small correlation was found

between both parameters and QA results [27]. Some specific treatment plan accuracy metrics like the SAS (Small Aperture Score) and MFA (Mean Field Area) were calculated in 2014. However, only the SAS revealed having a small correlation with QA results [28]. On the other hand, no correlation was found with SAS metric and MFA [29]. Several studies were made, but until now no relationship has been found between plan parameters and QA failure. In this project we intend to study some plan parameters such as number of MU, fields, and some metrics, such as the SAS and MCS in order to explore their usefulness as predictors of QA failure.

2.3.0.2 *In vivo* Dosimetry

The *in vivo* dosimetry concept consists of measuring the radiation that is delivered to the patient during his treatment. Then the measured dose is calculated for a few specific locations of the patient, in case of point dosimeters, or for the irradiated volume, by using EPID and mathematical models. Then, the measured dose is compared with the planned dose (calculated on the TPS) in order to ensure that the treatments are carried out as they were planned.

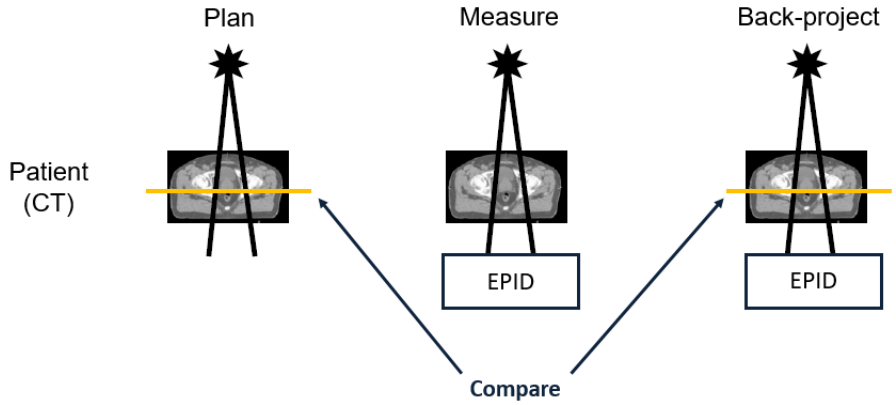

Figure 2.8: Schematic presentation of EPID *in vivo* dosimetry procedure.

This procedure is not only able to detect errors but also to assess quantitatively the dosimetric impact of the error. The error sources could be due to patient positioning and differences in patient anatomy such as weight loss or organs movement. Moreover, the treatment parameters could accidentally be modified between pre-treatment verification and the first fraction verification, which occurred in two of the 4337 patients analysed in NKI-AVL, Amsterdam [30]. In these cases pre-treatment QA was not enough, only *in vivo* dosimetry could detect this.

2.3.0.2.1 State of the Art The first studies of *in vivo* dosimetry for breast cancer patients were realized in 1991 using diodes [31]. In the following years several types of dosimeters were tested including TLDs (Thermoluminescent dosimeter) [32], radiochromic films [33], and MOSFETs (Metal Oxide Semiconductor Field Effect Transistor) [34]. However, the use of these dosimeters is limited by the fact that they obtain dose values for only a finite set of points and need to be placed manually on the patient's skin, which is inconvenient. Its replacement by EPIDs enables measuring the dose to the whole irradiated scan plane without increasing the time of treatment and without the need to be in contact with the patient [16].

In the first attempts to determine the dose *in vivo* with LI-FI (Liquid-Filled) EPID, the measured dose was achieved at the EPID level (positioned behind the patient/phantom). It therefore measured the exit dose, in other words, the beam radiation that was not absorbed by the patient [35]. In 1998 the dose at the mid-plane of patient was obtained, which is parallel to the EPID plane. The acquired images were then analysed by a back-projection algorithm that enables converting that dose at EPID level, to the dose inside the patient [36].

Over the years the LI-FI EPID has been replaced by the CCD-based EPID (Camera-based EPID), prompted by its slow acquisition of images, which avoids the instantaneous measurement of the dose received by the patient during treatment [37]. Despite the fast image acquisition, the visible photons that interact with the screen fluorescence of CCD-based EPID generate a signal not only at the correspondent pixel but also in the pixels around them [38]. Thus, the CCD-based EPID was replaced by the a-Si EPID (Amorphous silicon EPID), which is the EPID most widely used amongst radiotherapy centres.

In order to obtain a more realistic estimate of *in vivo* measurements, there was a growing need to measure the dose throughout the irradiated volume of the patient instead of measuring the exit or mid-plane dose. To do this, it was required to extend the back-projection model for several planes parallels to the mid-plane. The 3D EPID *in vivo* dosimetry is clinically implemented in NKI-AVL in Amsterdam and other few places.

2.4 EPID dosimetry

A portal image is acquired with the radiation obtained from the radiotherapy treatment. It was initially used for set-up position verification, as it shows the irradiated area. The portal images were initially acquired using films, but develop-

ment of EPIDs (Electronic Portal Imaging Device) enables digital image acquisition with a high level of accuracy. These features have led to an enhanced interest in introducing the EPID as a way to do the pre-treatment and *in vivo* dose verification.

2.4.1 EPID

The EPID is a device attached to the LINAC and placed at the opposite side of the LINAC's head, following its movement (Figure 2.9). It measures the intensity of the radiation delivered to the patient during treatment by acquiring portal images [39].

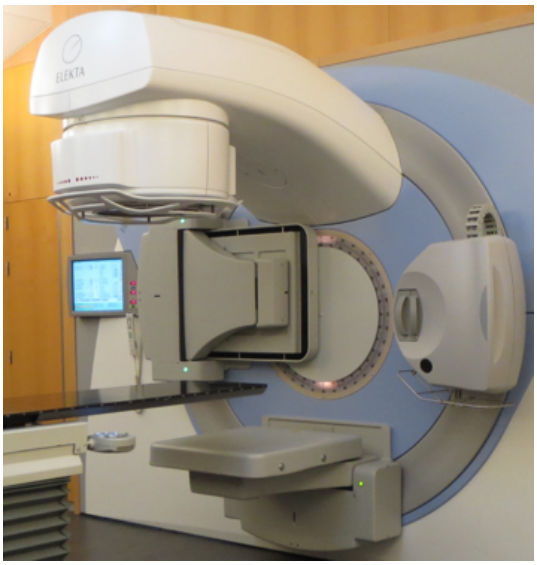

Figure 2.9: Elekta Synergy LINAC.

For clinical imaging it is necessary to apply some corrections to the acquired images in order to remove background noise and provide a spatially uniform response.

During the irradiation a frame (signal from one readout of the entire panel) is taken every two seconds, approximately. The EPID signal is calculated by multiplying the average pixel value by the number of frames acquired. Before obtaining the total EPID signal, each individual frame is corrected for individual pixel sensitivity and offset. The corrected image I_{proc} is giving by [40]:

$$I_{proc} = \frac{I_{raw} - I_{dark\_dyn}}{I_{flat} - I_{dark}} \tag{2.4}$$

Where the I_{raw} is the average of all frames or each frame individually, I_{dark_dyn} is a dynamic dark image acquired every 30 seconds when the EPID is not being irradiated. The I_{flat} is an open field image delivered to the entire sensitive area that accounts for individual pixel sensitivities (response) and corrects their differences. The I_{flat} and I_{dark} are acquired when EPID is installed or when some changes in the set-up are made. This correction is applied to the images automatically at the time of measurement with the IviewGT software. Variations in the dark field current introduce an offset to the pixel signal. This procedure was developed to optimize image quality [40], [41].

2.4.2 A-si EPID

The a-Si EPID (currently the most widely used EPID in radiotherapy centres) was first described by Antonuk et al. in 1996. It consists of a regular two-dimensional matrix of image pixels. Each pixel is one a-Si FET (Field-Effect Transistor), which is connected to a photodiode. Each pixel is connected to a gate and a data line that are arranged perpendiculary to each other as shown in Figure 2.10. The photodiode has a behaviour similar to the capacitor, as it allows light to be captured and stored in the form of electric current, and the FETs control the read-out of the recorded signal. An x-rays converter, which is located at the top of the matrix, is required and is a copper plate attached to a phosphor screen. The copper sheet is also responsible for absorbing the radiation that is diffused from the patient as the low energy radiation which otherwise would only reduce the image contrast [42].

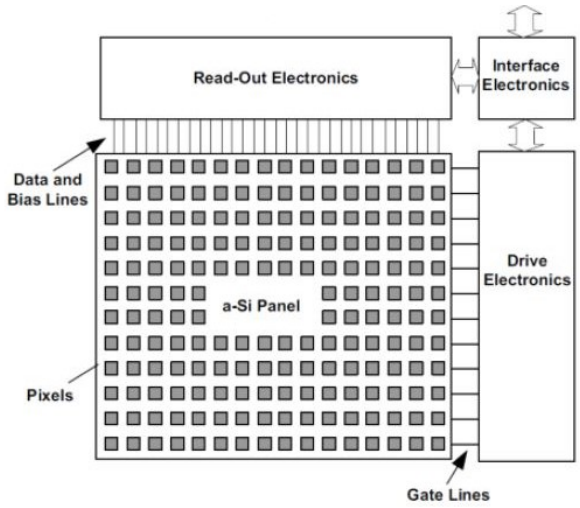

Figure 2.10: Representative scheme of a-Si EPID components [43].

Chapter 3

Materials and Methods

3.1 Clinical Implementation of EPID *in vivo* dosimetry

3.1.1 IviewGT

In order to provide the dose calculation, it is indispensable to acquire open fields of each patient, which are used to estimate the patient's transmission. The open fields are EPID images obtained for each field of the patient plan without an attenuating medium (patient or phantom). Furthermore, during the patient's treatment EPID images are acquired at the same time through IviewGT Software used for radiotherapy imaging. When attached to a LINAC, the system captures portal images that can then be viewed and stored. As described by R. J. W. Louwe et al. [44], it is recommended to wait around 30 seconds between the acquisition of two consecutive EPID images in order to acquire new dark images. However, according to the IviewGT manual and the parameters defined in the .ini file, the dark-field images are acquired continuously every 15 seconds when the EPID is not being irradiated. The waiting time is because after beam-off, the system waits 15 frames (around 2.5 frames per second) before acquiring a background offset image. The system needs to acquire 20 offset frames in order to obtain a dark image. This process is important, since the bias voltage could vary and will influence all frames acquired to perform an EPID image [45].

3.1.2 EPID calibration

The EPID calibration is an essential procedure for obtaining the parameters for the back-projection method. It establishes the dose-response relationship by relating

EPID pixel values to dose values. It is also required to obtain experimentally the scatter kernels (scatter within the EPID and scatter between patient to EPID) for different field sizes and for 6 and 10MV. Based on results of some test institutions, a new global calibration model was obtained and tested. As a result, in the last year doing this has become faster and instead of 8 hours of full measurements only 20 minutes are required.

This new procedure has the following steps:

1. Slab phantom

   A slab water phantom with 20cm thickness was used, as shown in Figure 3.1. Each slab phantom has 1 cm thickness and the middle one (2cm thickness) has a small hole to place the ionization chamber (IC) sensor in the centre of the phantom (isocentre). The reference field size (10x10 cm^2) and phantom thickness are chosen to be representative of clinical situations.

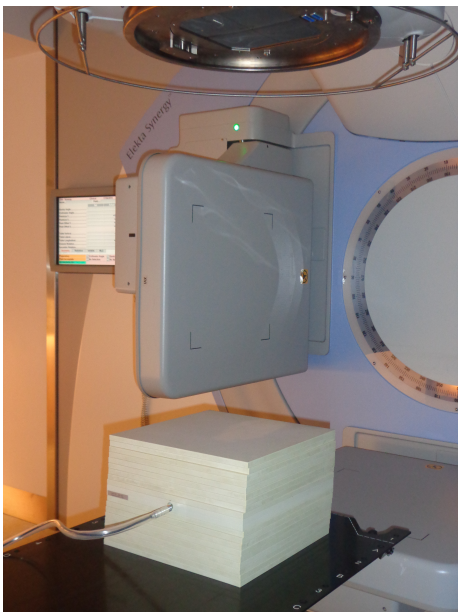

Figure 3.1: Assembly used in EPID calibration: Slab phantom with 20cm thickness and an IC located at the isocentre.

2. IC + Electrometer

   Before irradiating the phantom with a slab field (10×10) and measuring with the IC, it is necessary to accurately evaluate the temperature and pressure (Figure 3.2) conditions in the room in order to introduce these parameters in the electrometer. The ICs usually consist of a central electrode, an anode,

and the chamber wall is composed of a conductive material (cathode). The area bounded by the wall of the chamber is filled with gas at a relatively low pressure. A potential difference is established between the anode and the cathode in order to separate the gas ion pairs produced by ionization processes. This generates an electric current, which can be measured by the electrometer (Figure 3.3) [16].

Figure 3.2: Thermometer (model: HD 2307) and barometer (model: HD 2114B.O RTD) from Delta OHM company.

Figure 3.3: Compact ionization chamber (left) from IBA Dosimetry with serial number: 2380 and the electrometer (right) also from IBA Dosimetry.

IC measurements for 6MV and 10 MV were performed twice. The EPID measurements should ideally be acquired in the absence of a couch, hence with gantry at 90 degrees. However, it can be performed with gantry angle 0 degrees if the correct couch correction is used.

3. Sensitivity Matrix (S_{ij})

   An open portal image was acquired with 26×26 field size for 6 and 10MV. Such images are required for the calibration in order to describe the relative

sensitivity of each individual pixel in relation to the isocentre pixel.

4. Calibration Evaluation

   In order to check the EPID behaviour and the calibration, besides the 10×10 field size, the 5×5 field and 20×20 field with the respective open fields should be measured. Then, the PDapp is used to compare the measured dose and planned dose. By performing an EPID calibration every month, it is also possible to verify the EPID's reproducibility during that time.

   It is important to mention that every time the panel is re-calibrated, a new PDapp calibration model should be created with new values. Since the calibration procedure is a crucial step to obtain accurate results, every time the LINAC's output changes, a new calibration is needed.

3.1.3 PDapp Software

One hundred and ninetythree patients were measured *in vivo* (during the treatment) and analysed using a software called PDapp, which is developed by the Netherlands Cancer Institute Antoni van Leeuwenhoek (NKI-AVL). This software is not yet commercially available, and is still undergoing trial testing. The PDapp requires the EPID images (with and without a patient) for each field, patient's CT to determine the patient contours, the DICOM-RT Plan, DICOM-RT Structure and, RT dose that corresponds to the planned dose.

This software allows us to perform the dose evaluation in two different ways: using the EPID open fields method and using the EPID DRR (Digitally Reconstructed Radiograph) method, as described in the next chapter.

3.1.3.1 Back-projection Algorithm

The back-projection algorithm reconstructs the dose inside the patient/phantom from the portal image acquired by the EPID. Knowing that the EPID frame-averaged acquired images were previously multiplied by the number of frames and corrected by the dark and flat images, it is necessary to correlate the EPID pixel values to dose. In order to estimate the response of each pixel a sensitivity matrix (S_{ij} matrix) is measured, which describes the relative sensitivity of each individual pixel in relation to the isocentre. To correlate this information an IC is located in the centre of a phantom with 20cm thickness in order to measure the dose on the

central axis. This is done for the reference field size ($10\times10cm^2$). Under the same conditions, EPID images are acquired. The value measured is then correlated with the intensity of the EPID pixels.

Besides the radiation reaching the EPID directly, there are some factors that contribute to differentiate the EPID dose (D_{ij}^{EPID}) and the dose actually received (PD – Portal Dose). Since there is scatter within the EPID, the relation between the dose at certain pixel ij of the EPID and the dose image after correction for lateral scatter is given by:

$$D_{ij}^{EPID} = PD_{ij}^{EPID} + Sc_{ij}^{EPID} \tag{3.1}$$

Where Sc_{ij}^{EPID} is the scatter within the EPID and is given by the convolution between PD_{ij}^{EPID} and the scatter kernel K_{ij}^{EPID}.

Another factor that must be corrected is the scatter from patient to EPID. In this sense, the PD is given by:

$$PD_{ij}^{EPID} = Pr_{ij}^{EPID} + Sc_{ij}^{patient\rightarrow EPID} \tag{3.2}$$

Where the primary portal dose (Pr_{ij}^{EPID}) is the radiation coming directly from the head of the LINAC and $Sc_{ij}^{patient\rightarrow EPID}$ is the scatter contribution from patient to EPID. In order to obtain the latter component one first calculates the total transmission T_{ij}^{total}, obtained by dividing the PD with patient by the PD without the patient (open field):

$$T_{ij}^{total} = \frac{PD_{ij}^{withpatient}}{PD_{ij}^{withoutpatient}} \tag{3.3}$$

The scatter contribution is estimated by joining equations 3.2 and 3.3 in order to separate into primary transmission, when no scatter from patient would reach the EPID ($T_{ij}^{primary}$), and the scatter contribution:

$$T_{ij}^{total} = \frac{Pr_{ij}^{withpatient} + Sc_{ij}^{patient \rightarrow EPID}}{PD_{ij}^{withoutpatient}} = T_{ij}^{primary} + \frac{Sc_{ij}^{patient \rightarrow EPID}}{PD_{ij}^{withoutpatient}} \tag{3.4}$$

The scatter contribution is determined, knowing that the T_{ij}^{total} depends on field size, but $T_{ij}^{primary}$ has to be size independent. Therefore, T_{ij}^{total} is experimentally obtained as a function of field size by irradiating a phantom of a reference thickness (20 cm) with square field of different sizes. Thus the $T_{ij}^{primary}$ component is given by:

$$T_{ij}^{primary}(fs^2) \approx \lim_{fs \rightarrow 0} T_{ij}^{total}(fs^2) \tag{3.5}$$

After estimating the scatter components within the EPID and patient→EPID, we are able to calculate the dose inside the patient. To do that it is essential to determine the scatter within the patient in order to obtain the dose at different planes, perpendicular to the beam. Since the algorithm does not take the inhomogeneities into account, we are faced with a homogenous medium. As a consequence, the radiological pathlength is approximately equal to the geometrical pathlength, and this is obtained by using the 3D contour information from the patient CT.

The reconstructed dose ($\mathrm{D}_{ij}(d_{reconst})$) is given by:

$$D_{ij}(d_{reconst}) = Pr_{ij}(d_{reconst}) + Sc_{ij}(d_{reconst}) \tag{3.6}$$

Where $d_{reconst}$ is the distance of the reconstruction plane, which is parallel to the EPID, from the accelerator target and $Sc_{ij}(d_{reconst})$ is the scatter contribution within the reconstruction plane. The $Sc_{ij}(d_{reconst})$ depends on the radiological thickness of the patient and accounts for the field-size dependence (K^{mid}) of the scattered dose in the reconstruction plane. First, the $Pr_{ij}(d_{reconst})$ is weighted with the scatter thickness dependence. Then, the result is convolved with the scatter kernel (K^{mid}.

To calculate the $\mathrm{Pr}_{ij}(d_{reconst})$, the inverse square law (ISQL) and an attenuation correction (AC) are applied:

$$Pr_{ij}(d_{reconst}) = Pr_{ij}^{EPID} \times ISQL \times AC_{ij}(d_{reconst}) \tag{3.7}$$

$$ISQL = \left(\frac{d_{reconst}}{d_{EPID}}\right)^{-2} \tag{3.8}$$

Where d_{EPID} is the distance of the EPID from the LINAC target and equals 160cm for our EPID. The attenuation depends on the radiological path length of a ray through the patient from the reconstruction plane to the exit surface. First, it is important to estimate how the $T^{primary}$ changes in the patient with depth:

$$\tilde{T}^{primary}(d_{ij}^{radiol}) = exp[-\mu_{AC}(d_{ij}^{radiol}) \tag{3.9}$$

Thus, the AC is given by:

$$AC_{ij}(d_{reconst}) = \tilde{T}^{primary}(d_{ij}^{radiol})/T^{primary} \tag{3.10}$$

Finally, the 3D dose distribution is calculated by changing the distance $d_{reconst}$ of the reconstruction plane between a minimum and a maximum value for each gantry angle [39], [46].

The treatment couch is a source of error that can attenuate the beam before it irradiates the EPID. In relation to the study group (breast cancer patients) a couch correction is applied when the gantry angle has a range of -41 to 41 degrees. The Correction Factor (CF) is given by the next formula:

$$CF = \frac{\alpha}{\cos(\theta)} \tag{3.11}$$

Where α is the attenuation coefficient of the table and θ is the gantry angle. The couch absorption is 3.2% and 2% for 6MV and 10MV respectively. Note that oblique beams have larger absorption.

3.1.3.2 DRR Method

With the intention to simplify the EPID *in vivo* procedure, we studied the DRR option of PDapp. This option allows us to perform dose calculation analysis without taking open fields, which makes the procedure much faster. The only difference between EPID open fields and DRR methods is the way to obtain/estimate the primary transmission ($T^{primary}$). Therefore, $T^{primary}$ is obtained by:

$$T^{primary}(t_{ij}) = exp(-\mu_{AC}.t_{ij}) \tag{3.12}$$

Where μ_{AC} is the linear attenuation coefficient of water for a specific beam energy and t_{ij} is the radiological thickness. t_{ij} is determined by tracing ray lines from a virtual source through the patient's CT scan (DRR). Then, all the relative electron density values (CT numbers) are replaced by the corresponding values for water [39], [47].

The measured dose is then compared with the planned dose through gamma evaluation (with 3%, 3mm criteria).

3.1.4 Dose Comparison

The gamma evaluation is currently the most straightforward method for comparing two dose distributions, since it takes both dose and spatial difference into account. The calculated distribution will be a benchmark measurement to compare to the measured dose distribution.

3.1.4.1 DTA (Distance-to-Agreement)

The DTA is the spatial distance between a point in a calculated distribution $\vec{r_c}$ and the closest point in the measured distribution $\vec{r_m}$ that exhibits the same dose:

$$DTA(\vec{r_c}) = min|\vec{r_c} - \vec{r_m}| \tag{3.13}$$

This is done for each evaluated pixel. The threshold value is usually $\Delta d = 3mm$, which means that if the DTA exceeds Δd the comparison fails. On the other hand,

if the DTA is less than Δd the comparison passes at this specific point [48].

3.1.4.2 Dose Difference

The dose difference analysis is the point-by-point comparison between the reference distribution $D_c(\vec{r_c})$ and the evaluated distribution $D_m(\vec{r_m})$ according to:

$$\Delta D = D_c(\vec{r_c}) - D_m(\vec{r_m}) \tag{3.14}$$

As in the DTA method, the dose difference tool also uses a passing criterion that is usually 3%, which means that if the measured and planned dose differ by 3% or less, the measured dose passes the test for this point [49].

3.1.4.3 Gamma Evaluation

The gamma evaluation method combines the features of dose difference and DTA methods, which complement each other. An ellipsoid is used as the surface representing the acceptance criteria. Knowing that r represents the spatial location and δ the dose difference between the evaluated and reference distributions at the point r_m and r_c respectively. Thus, the gamma evaluation is given by:

$$\Gamma(\vec{r_c}, \vec{r_m}) = \sqrt{\frac{r^2(\vec{r_c}, \vec{r_m})}{\Delta d^2} + \frac{\delta^2(\vec{r_c}, \vec{r_m})}{\Delta D^2}} \tag{3.15}$$

Where $r(\vec{r_c}, \vec{r_m}) = |\vec{r_m} - \vec{r_c}|$ is the spatial difference between the position of the reference point and the evaluated point and $\delta(\vec{r_c}, \vec{r_m}) = D_m(\vec{r_m}) - D_c(\vec{r_c})$ represents the difference between the evaluated dose distribution D_m at position $\vec{r_m}$ and the reference distribution D_c at position $\vec{r_c}$.

Each measured point is evaluated to determine if both the dose difference and DTA exceed the selected tolerance. The origin is placed at the reference point (its position and dose). The ellipsoid corresponds to the region where the measured point passes both dose comparison (ΔD) and DTA (Δd) methods. Thus, the gamma value is given by:

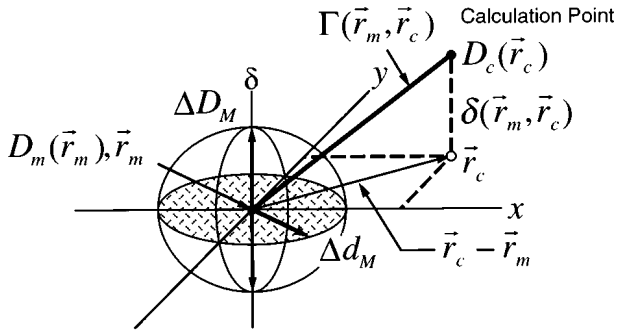

Figure 3.4: Geometric representation of Gamma evaluation method using the combined ellipsoidal dose-difference and DTA tests. The x and δ axes represent the spatial location r_c of the reference point relative to the evaluated point. The vertical axis (δ) represents the dose difference between the measured $D_m(r_m)$ and the reference $D_c(r_c)$ position [50].

$$\gamma(\vec{r_c}) = min\{\Gamma(\vec{r_c},\vec{r_m})\}\forall\{\vec{r_m}\} \tag{3.16}$$

Therefore and according to the chosen criteria (in general 3%,3mm), the radius is normalized and the pass-fail criterion becomes:

$$\gamma(\vec{r_c}) \leq 1, \text{calculation passes,} \tag{3.17}$$

$$\gamma(\vec{r_c}) > 1, \text{calculation fails.} \tag{3.18}$$

Therefore, if γ is less than one it means that both distributions agree for that point with respect to the chosen criteria [50].

Another important parameter used to compare two different distributions is gamma passing rate ($\%\gamma < 1$), which is a specified isodose line that has γ values smaller than 1. The threshold currently used at the clinic for the ArcCHECK pre-treatment measurements is $(\%\gamma < 1) > 90\%$.

3.1.4.4 PDapp's Layout

The reconstructed dose distribution is then compared with the corresponding reference dose distribution. Before performing the gamma analysis it is important to

check if the portal dose and the planned dose are matched, since the EPID position is variable. In case of interlock (LINAC's break) several images are stored for the same field that must be grouped, otherwise the software does not take into account the total dose received. The interlocks are another study case, since it appears that sometimes the system is not able to acquire the remaining dose, which would result in an EPID under-dose.

Usually a fraction analysis is performed, which evaluates all fractions independently and gives a summary result according to the results obtained in each fraction. The gamma evaluation is based on gamma passing rate ($\%\gamma < 1$), gamma mean (γ_{mean}), and dose difference at reference point (D_{ref}). The reference point lies at or near the centre of the target volume. In case of doubts with certain results it is useful to perform a 2D or 3D analysis, which gives us a perspective of what is happening with each field individually.

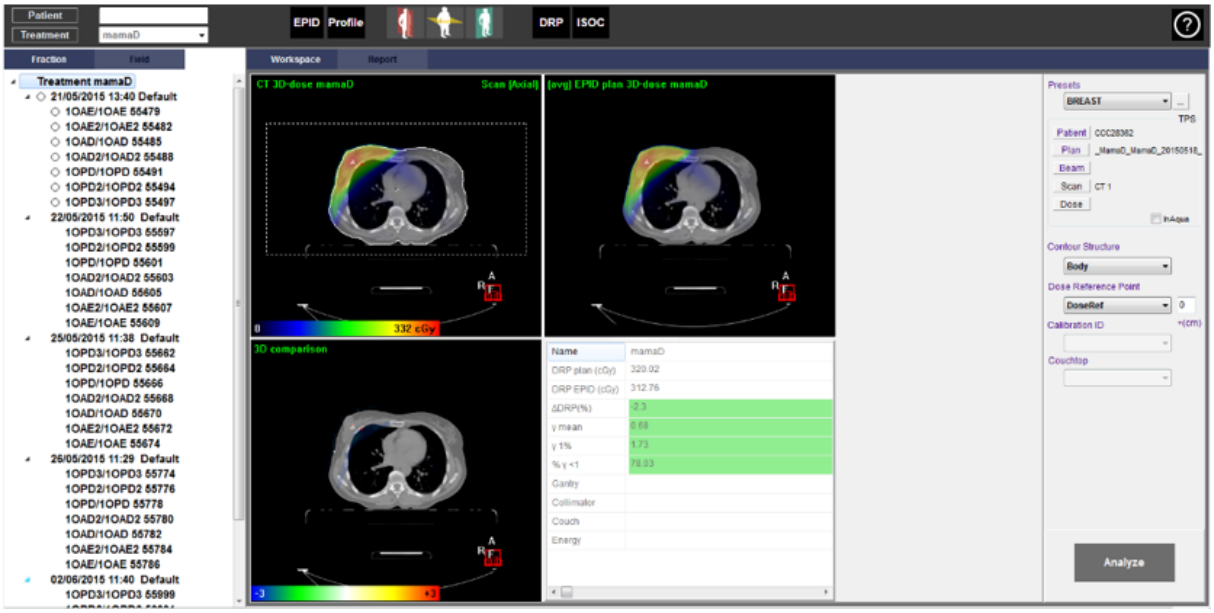

Figure 3.5: PDapp software layout.

Initially it is important to have an idea about the PDapp's layout and the tools that it can use and display. Figure 3.5 shows the layout of PDapp software. On the left side all patient's fractions are represented with the corresponding fields measured by the EPID. Note that the first fraction stands out from the others because it is the open field fraction. In the centre are the 3D total planned and measured doses respectively, on a patient's CT. If we click on a specific field it shows these doses field by field. Below these two images is a compound image with the difference between the planned and the measured images in terms of gamma comparison. It

is important to mention that a gamma of 2, which has a red colour, implies an overdose, while a -2 gamma indicates an underdose, represented by blue colour. On the right side of the compound image we see the summary results of gamma evaluation fraction-to-fraction or the total evaluation, depending on what we intend to analyse. It is also possible to see the profile between the measured and the planned dose along the isocentre plan.

Another important tool is the Portal Image Viewer, which enables us to see and overlap the boundaries of the planned and measured fields.

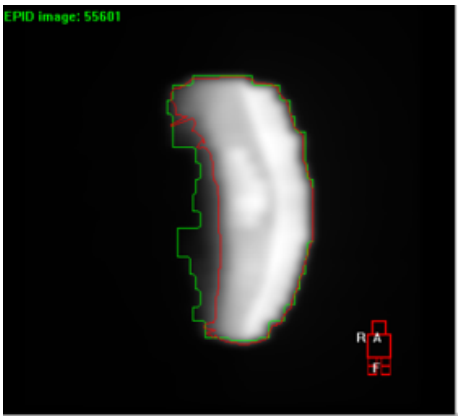

Figure 3.6: Portal Image Viewer: Contours representation of the planned OPD field and the corresponding portal image.

Before performing the analysis, a match between the EPID and the planned image should be done (Figure 3.6). The software performs the match automatically but sometimes the images do not look aligned, which influences the results since the PDapp is comparing points that do not correspond to the same place. In these cases, the software allows us to perform the match manually and make the adjustments to the portal image.

3.1.4.5 PDapp's Reports

When the software performs the gamma evaluation, it gives us the possibility to show how the fields look in terms of gamma analysis by differentiating on a colour scale. It is also possible to see the couch correction that was applied to make the dose calculation, the number of fields, the calibration used, and if the analysis was performed by EPID or DRR transmission.

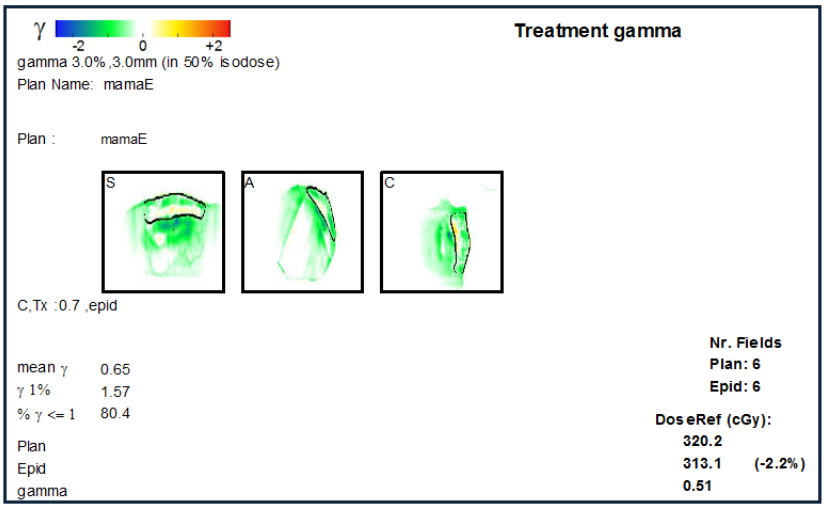

Figure 3.7: 3D EPID *in vivo* dosimetry report for a breast cancer patient.

Generally the first, second, third and the last *in vivo* fractions are measured. The software presents the four fractions results and a synthesis result that takes into account the results of the four fractions (fraction analysis - Figure 3.7).

For treatment evaluation it is usual to use the 3D report, since it gives us an overview of how the treatment went. However, if there are some uncertainties about the results and consequently about the treatment, the analysis is performed field by field at the isocentre plan (2D report - Figure 3.8).

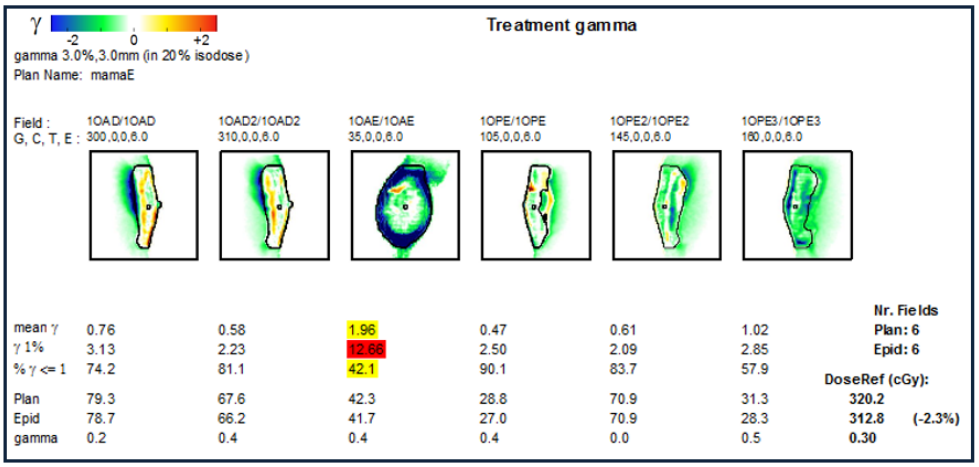

Figure 3.8: 2D EPID *in vivo* dosimetry report for a breast cancer patient.

3.1.4.6 Clinical *in vivo* Threshold Values

After analysing a significant sample of patients and in order to clinically implement the EPID *in vivo* dosimetry it is essential to define the acceptable threshold values for γ_{mean}, $\%\gamma < 1$, and D_{ref} parameters. The determined values are used to decide if the patient's treatment can proceed or if something went wrong and should be corrected before another fraction. The threshold values were estimated by using two different methods, the Quartile Method and SD (Standard Deviation) Method, and were applied for first fraction results, for the average of the first three fractions, and for the best of three fractions. For the Quartile Method, we calculate the first and third quartiles of the three data sets and the IQR (Inter-Quartile Range) by subtracting quartile 1 from quartile 3. The interval is obtained by estimating the lower and upper limits according to this formula:

$$LowerLimit = Q_1 - (1,5 \times IQR)$$
$$LowerLimit = Q_3 - (1,5 \times IQR)$$

All values that do not belong to the range are considered outliers.

The SD Method uses measurements (Mean and SD) that are highly affected by extreme values. It is defined as:

2D Method: Mean $\pm$2SD
3D Method: Mean $\pm$3SD

The observations outside these intervals may be also considered as outliers [51].

It is important to notice that for γ_{mean} the upper limit was considered as a threshold, for $\%\gamma$ <1 the threshold is the lower limit.

3.1.4.7 Impact evaluation of some error sources

When there is an error detected by the EPID, the source is not always known. Assuming that the correct treatment plan was sent, as each specific parameter was previously checked by pre-treatment QA, it is useful to study the impact of a LINAC's output variation in EPID evaluation. As a part of routine LINAC QA, the output is measured daily for each energy. In order to study this parameter variation on EPID results, we measured the dose received by the EPID with an IC during the EPID calibration. Following that procedure, this measurement is used to relate pixel intensity to dose values, and is increased and decreased by 1, 2, and 3%. These changes are accompanied with a PDapp analysis and the EPID's sensitivity

evaluation.

As mentioned above, a LINAC's error is usually accompanied by a sudden halt in irradiation. After that break the treatment must be resumed at the point it was before the beam-off. We decided to investigate if there was a relationship between the interlocks and the EPID results, since it occurs with some frequency.

3.1.4.8 EPID dosimetry vs ArcCHECK

Before implementing the EPID pre-treatment and *in vivo* QA, it is important to compare these measurements with the device (ArcCHECK) currently used by the clinic to perform pre-treatment QA. Thus, we measured 197 patients *in vivo*, 30 patients with the ArcCHECK detector (Sun Nuclear Corporation), and EPID using the ArcCHECK as a phantom. We compared the results differences between *in vivo* and pre-treatment results. In relation to pre-treatment, we also compared the results obtained with the two different devices (AC and EPID).

3.2 EPID dosimetry for pre-treatment QA

In an attempt to study the possibility of replacing the ArcCHECK pre-treatment QA by EPID, a software was developed that compares the measured dose and the planned dose before treatment. The measured dose was obtained by measuring the patient's fields without any attenuator medium (open fields), which are already required for the *in vivo* evaluation. This version was first developed in an attempt to study the possibility of obtaining reliable results. The EPID portal doses are obtained directly from the intermediate step of PDapp, which converts each pixel intensity to dose. Since the dose comparison is performed at EPID level, the planned dose was re-calculated in Monaco 100 cm away from the source, in other words, as close to the EPID (located 160 cm away from the source) as possible. Besides this feature, a reference phantom (20x20cm^2) was used forcing a density of 3 g/cm^3 and with gantry override (Figure 3.9).

The choice to triple the density of water (major constituent of human beings), was to simulate the same effect that occurrs in the Cu (3mm) build-up layer of EPID. In this specific case it allows that the maximum dose achieved in build-up region reaches its maximum at a lower depth (Figure 3.10). Consequently, and knowing that the planned dose was calculated with a Monte Carlo algorithm with 3% of precision, the first slice of 3mm is considered as build-up material and the

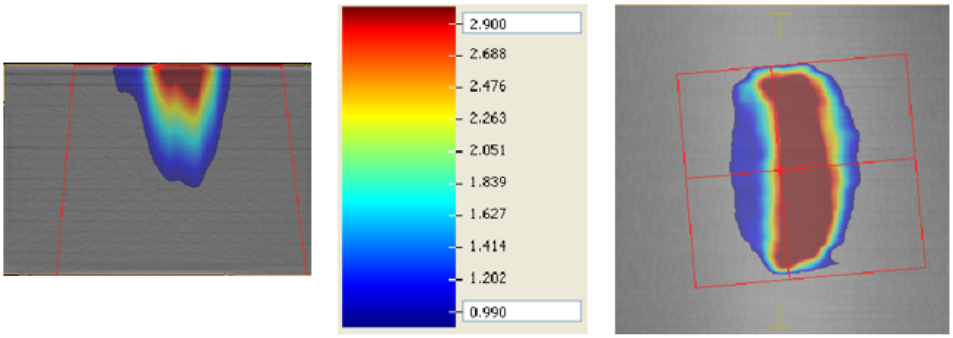

Figure 3.9: Clinical plan re-calculated (axial – left and sagittal planes – right) in square slab phantom in Monaco. The colour scale (centre) represents the dose in Gy.

second slice (3mm-6mm) corresponds to the maximum response (highest dose).

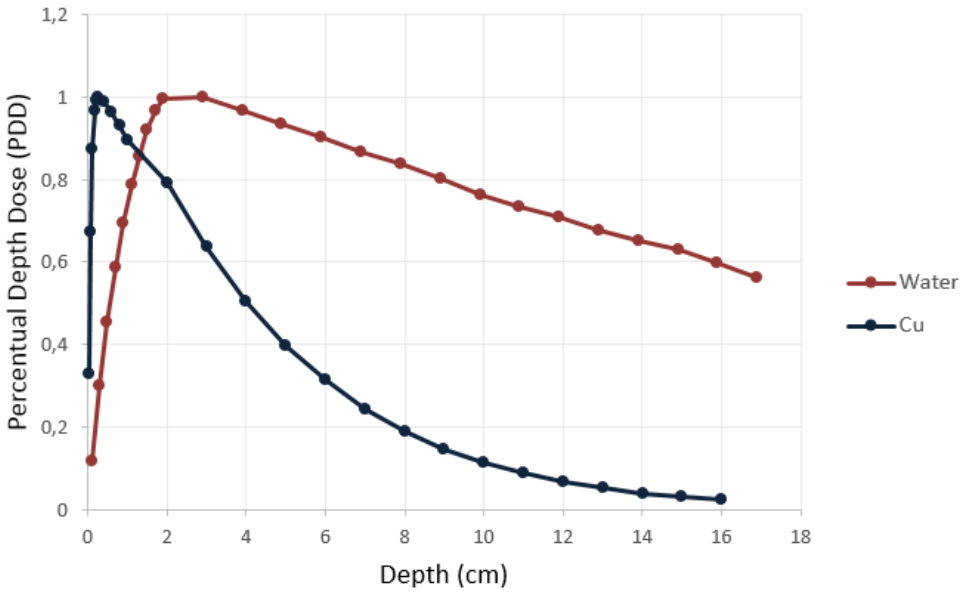

Figure 3.10: Penelope Simulation. Comparison between the PDD and depth for water and Cu for a 6 MV photon beam.

Both images were then analysed at pixel level for each field of treatment plan, and a gamma analysis was performed. 10 IMRT and 9 VMAT plans were re-calculated and compared with the corresponding measured portal dose images.

3.2.1 RTP File Analysis

This study aims to identify one or more IMRT treatment plan parameters or metrics, that could be used to identify plans that were likely to fail in pre-treatment QA.

3.2.1.1 RTP Files

The RTP file contains all the needed information for the ELEKTA LINAC to deliver the treatment effectively. Besides the basic information about the patient such as the ID, plan name and patient's name, it also has the number of MU (Monitor Units), gantry angle, and the position of the MLC's leaves per CP (Control Point). The CP defines the position of each particular leaf at a specific fraction of the total MU. A MU is a measure of LINAC output, in other words it is the radiation delivered during beam-on per time. The output is verified by radiation detectors that are located in the LINAC's head in order to monitoring the dose rate [16].

Depending on the geometry of the relevant structures of the plan, the TPS will create a more or less complex set of fluence maps for the plan. The more complex the beam is, the greater is the possibility that the delivered absorbed dose will differ from the desired one. Although the TPS takes into account the mechanical limitations of the delivery systems, they may sometimes still be too complex for the delivery system. For that reason it is extremely useful to find a relationship between the treatment parameters and the QA results. Using a metric that is strongly correlated with treatment plan would help to avoid these specific parameters which will decrease the time required for pre-treatment QA. Thus, the last part of the project was to investigate the possible link between the IMRT plans and the pre-treatment QA's failure. By identifying a specific parameter in an IMRT plan that contributes to a treatment failure, it could reduce the LINAC time required for QA testing and contribute to the efficiency improvement of the treatment planning process. This study used the results of pre-treatment QA measurements with ArcCHECK detector, for a sample of 203 IMRT breast plans, planned with Monaco TPS (with pencil-beam algorithm), with Elekta Sinergy LINAC.

As explained above, the EPID detector is much more sensitive and accurate than the ArcCEHCK. Therefore, the RTP file measurements were also performed with EPID for 23 IMRT treatment plans. In order to do that, the treatment plan was delivered to the ArcCHECK phantom while the EPID acquired the portal images (Figure 3.11). The acquisition of open fields per field and per treatment plan was also required in order to perform the dose comparison with PDapp. The gamma evaluation was obtained with PDapp software after importing the respective patient

plan calculated in ArcCHECK phantom (Figure 3.12).

Figure 3.11: Mounting scheme of the EPID dose measurement in ArcCHECK phantom.

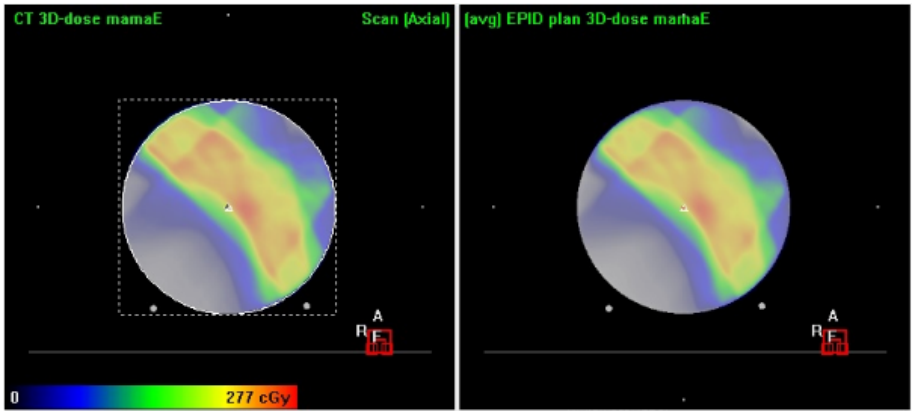

Figure 3.12: Comparison between patient plan calculated in ArcCHECK phantom (planned dose) with Monaco software and portal dose reconstructed inside the ArcCHECK phantom (measured dose).

The treatment plans were exported from the planning system in RTP file format for analysis. The 267 files were analysed using a home-written Python tool and some additional individual parameters including the number of control points (CP), the number of monitor units (MU), number of fields, number of segments and segment field size were obtained and written in a txt file.

As mentioned above, in the case of IMRT with MLC in dynamic mode, the MLC is acquiring different shapes while the beam is on. However, for some fields

it is necessary that the beam turns off in order for the MLC to acquire the desired conformation. To access the number of MU delivered at each CP, we used the Monitor-Units parameter in RTP file. This parameter varies between 0 and 1 in each field and describes the cumulative fraction of MU delivered. When a change in segment occurs, at this CP the number of MU-Units does not change. Therefore the number of segments was obtained by counting the number of times the dose delivered between consecutive CP was the same. In order to calculate the distance between opposite leaves it was necessary to know that the MLC used is asymmetric.

However, the study of the parameters such as the area per field and the number of small subfields does not take into account the weight of MU's per field. A small field with a higher dose has a greater weight than a small field with a lower dose. For that reason, another variable named SAS (Small aperture score) was studied that calculates the proportion of open leaf pairs that were separated by less than a given threshold distance. SAS is given by the next formula [29]:

$$SAS = \sum_{i=1}^{I} \frac{N(0 < a < x)_i}{N(a > 0)_i} \times \frac{MU_i}{MU_{beam}} \tag{3.19}$$

Where x is the aperture criterion, I is the number of fields, N is the number of leaf pairs not positioned under the jaws and a is the aperture distance between opposing leaves.

Another parameter obtained from literature is MCS, which takes into account the relative variability on leaf positions, the area of the beam opening, and the number of MU. The Leaf Sequence Variability (LSV) considers the position differences of each adjacent MLC leaf between consecutive CPs. Therefore, it characterizes the variability in segment shape by including all the moving MLC leaves (N) not positioned under the jaws and the coordinates of leaf positions (pos) [27]:

$$LSV_{segment} = \left\langle \frac{\sum_{n-1}^{N} (pos_{max}) - (pos_n - pos_{n+1})}{N \times pos_{max}} \right\rangle_{l\_bank} \times \left\langle \frac{\sum_{n-1}^{N} (pos_{max}) - (pos_n - pos_{n+1})}{N \times pos_{max}} \right\rangle_{r\_bank} \tag{3.20}$$

pos_{max} is the maximum distance between positions for a leaf bank and $\text{pos}_n - pos_{n+1}$ is the difference between adjacent MLC leaves for each bank.

The aperture area variability (AAV) is defined as the variation in segment area relative to the maximum aperture of opposing leaves in each CP:

$$AAV_{CP} = \frac{\sum_{n=1}^{N} (\langle pos_n \rangle_{left\_bank} - \langle pos_n \rangle_{right\_bank})}{N \times (\langle max(pos_n) \rangle_{left\_bank} - \langle max(pos_n) \rangle_{right\_bank})} \tag{3.21}$$

Then the relative segment weight is incorporated into the final complexity score:

$$MCS_{beam} = \sum_{i=1}^{I} AAV_{segment_i} \times LSV_{segment_i} \times \frac{MU_{segment_i}}{MU_{beam}} \tag{3.22}$$

Where I is the number of segments in the beam. The total plan complexity is the sum of all the MCS_{beam} weighted by the relative MU of each beam in the plan:

$$MCS_{plan} = \sum_{j=1}^{J} MCS_{beam_j} \times \frac{MU_{beam_j}}{MU_{plan}} \tag{3.23}$$

Where J is the number of beams in the plan.

Therefore, SAS and MCS parameters were calculated for each segment whose weight is in agreement with the number of MU delivered respectively. A value of 1 indicates that all leaf pairs in each segment have an aperture less than the given criterion for SAS.

These results were subsequently compared with QA results evaluated by ArcCHECK and EPID devices and the graphs are plotted. The QA analysis were performed with gamma criterion of 3%/3mm and dose threshold of 50%, which means that the volume corresponding to at least 50% of the prescribed dose (QA50) was evaluated.

Any binding found would be very useful for the actual ArcCHECK pre-treatment QA, but also when the EPID pre-treatment QA is implemented.

Chapter 4

Results and Discussion

4.1 EPID *in vivo* Dosimetry

4.1.1 EPID calibration

The EPID calibration is a procedure that is essential to obtain reliable results. It allows us to correlate grey values in the EPID image to the correct dose. For that reason, each time the EPID changes, it is mandatory to perform a new calibration.

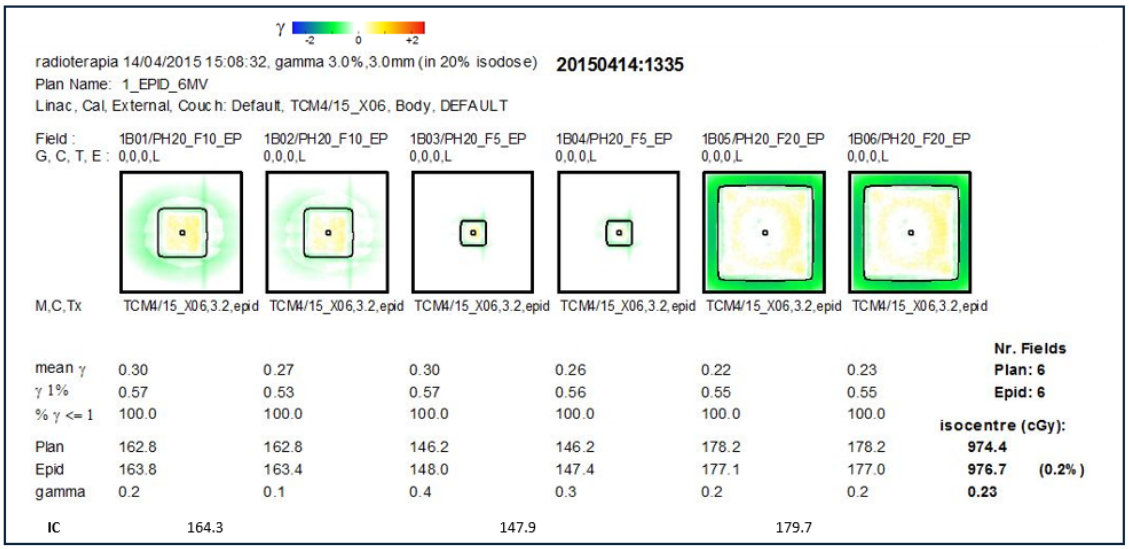

Figure 4.1: EPID calibration of April 2015 for 6 MV.

Before applying the new EPID calibration in patient cases, it is advisable to test it in the simplest cases. We used a slab 5×5, 10×10, and 20×20 fields in a slab

phantom 20 cm thickness and compared the measured and planned dose, by PDapp.

Figure 4.1 shows an example of a successful 6 MV calibration. All fields have 100% of $\%\gamma < 1$ and the γ_{mean} values are around 0.25. In relation to dose difference at the isocentre the planned and the measured dose have an overall difference of 0.2%, where the EPID measured a slight overdose. Comparing the measured dose with the IC, for the 10×10 and 5×5 fields, it is found that they are very similar. To the larger field (20×20), the IC dose differs not only from the measured but also from the planned dose. It was expected that the IC dose was equal to the EPID, at least for $10 \times 10 cm^2$ field size. However, the delivery of the planned dose is dependent to the LINAC output, which can explain these small variations.

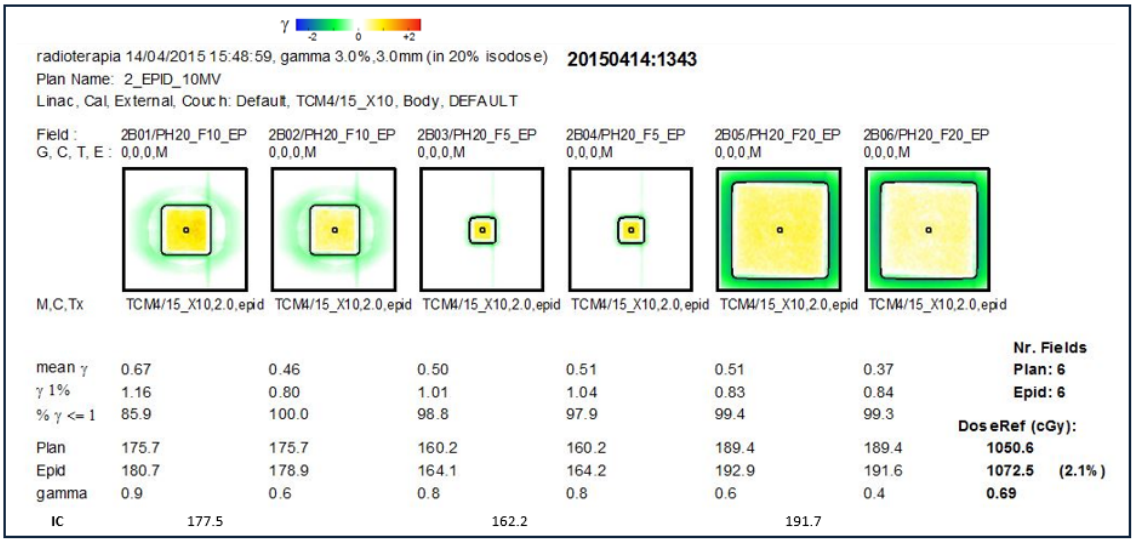

Figure 4.2: EPID calibration of April 2015 for 10 MV.

On the other hand for 10 MV calibration (Figure 4.2) the results are not in agreement with those expected since the γ_{mean} has a high value for simple squared fields (around 0.5) and the $\%\gamma < 1$ parameter should be 100% for all fields. In relation to $Dose_{ref}$ we see that the planned and measured dose differ by 2.1%, which is, once again, a large difference. However, for the reference field size (10×10) the IC measured 177.5 cGy at the isocentre, the planned dose is 175.7 cGy, and the EPID dose is 178.9 cGy. Contrary to the 6 MV results, for 10 MV the IC values are constantly between the planned and the EPID measurements with the exception of the last field (20×20 field size). While the greater variation between the planned and the IC for 6MV is 0.84%, for 10MV the variation is 1.24%. This fact could be explained by the fact that the LINAC output for 10MV has a greater day-to-day variation than

6MV. On the other hand, it was expected that the dose measured by the EPID was similar to the IC for the reference field size, since during the calibration the pixel value corresponded to the dose measured by the IC.

4.1.2 PDapp's reports

The PDapp reports allow the user to assess how effective the delivery of the dose was. According to the acceptance criterion defined (3%,3mm), it is considered that the treatment went as expected or that it is necessary to re-calculate the plan. This is an extremely useful tool that makes it possible to estimate the effect of immobilization devices or the anatomical changes when a specific underdose or overdose occurs.

The below figures show the difference between 2D and fraction (3D) IMRT dose verification.

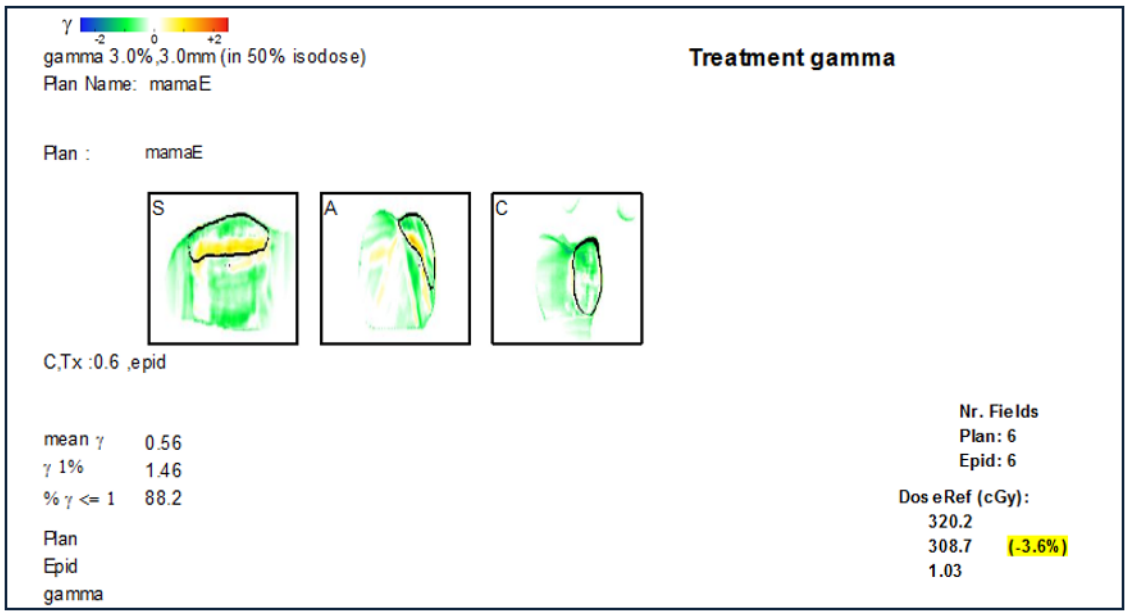

Figure 4.3: 3D PDApp Report.

The 3D report (Figure 4.3) shows a single synthesis result for the compound field, which means that it takes into account all treatment fields by giving the weight according to the delivered dose. The images displayed are the sagittal, axial, and coronal orientations respectively of the compound field.

Analysing the results we obtained a $\%\gamma < 1$ of 88,2% and a γ_{mean} of 0.56, which is a very good result for an *in vivo* measurement and for a breast cancer case. The D_{ref} difference, as expected, has an underdose of -3.6%.

Despite the good results it is important to have an idea of what happens with the fields individually at the reference plan.

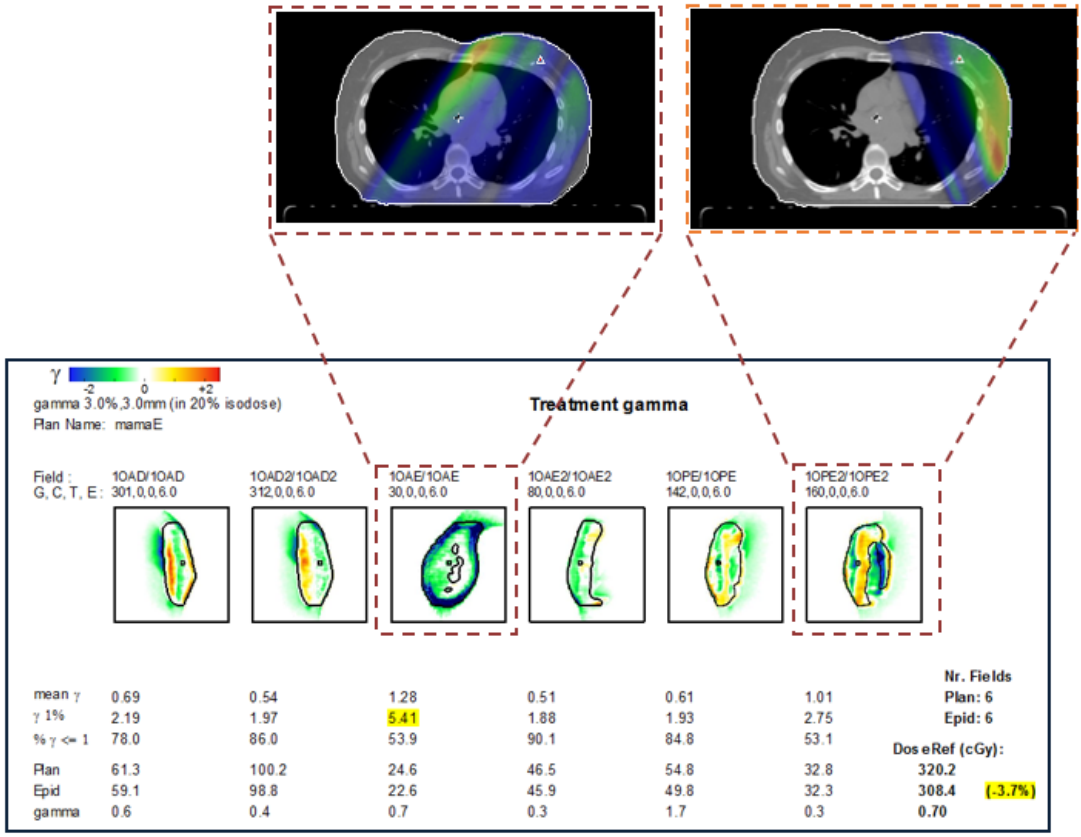

Figure 4.4: 2D PDApp Report.

The 2D report (Figure 4.4) makes an evaluation at the reference plan and presents the results field-by-field. Despite the good results obtained in the 3D report, it can be seen that there are two fields (OAE and OPE2) that have a $\%\gamma < 1$ and γ_{mean} much worse than the other ones.

In all 2D reports there are two fields that are worse than the others. We think that this occurs in the fields in which radiation crosses a larger area of the lung (OAE), since the back-projection algorithm does not take inhomogeneities into ac-

count and considers that the patient consists entirely of water. On the other hand, there are fields in which the radiation crosses the treatment table first (OPE2). As a result, not only the patient but also the EPID receives less radiation than expected.

Comparing the results obtained between 2D and 3D reports (Figures 4.4 and 4.3 respectively) it is noted that in most of the cases the γ_{mean} value is significantly greater for 2D analysis. It means that 2D dose deviations might be diluted in the total 3D dose distribution and possible anatomical changes or patient's movement no longer be detected. Thus, performing a 3D evaluation over all fields per fraction as opposed to 2D evaluation, field-by-field, has the advantage of time saving by avoiding false positives. For that reason the 3D report is always performed and if some doubts arise, 2D reports are analysed.

4.1.3 Time Trend

Figure 4.5 plots the EPID *in vivo* results from November 2013 until April 2015. We measured 193 EPID *in vivo* patients, and the results were evaluated through gamma analysis (γ_{mean}, $\%\gamma < 1$ and D_{ref} parameters). A time trend was created in order to evaluate the EPID behaviour over time (Figure 4.5). We compared the EPID *in vivo* results in terms of γ_{mean} (left vertical axis) and D_{ref} (right vertical axis) parameters, as the LINAC output (right vertical axis) and a possible link between these variables was studied. Since the output varies every day, a possible relationship between those variables was studied, as its impact on EPID results. Analysing the Time Trend (Figure 4.5) it is possible to see that the 3D γ_{mean} increases over time as D_{ref} decreases, with the exception of September 2014. The good results obtained between January to March 2014 were partly because the old version of PDapp (Pdose) was used. While PDapp presents the mean of the four fractions, the Pdose exhibits the results of the best fraction.

The LINAC's output is a variable that has small daily changes and since the EPID is a very sensitive device, this will affect EPID results. Until July the output of the LINAC has a deviation of +1%, which positively influenced the results. From November until the present, the LINAC's output has been around -1%, which helps to decrease the patient results (γ_{mean} are increasing and dose difference decreasing).

The LINAC interlocks are a problem that occurs from time to time. This problem happened with greater frequency during November 2014 and seems to be another source of error, which helps to increase the underdose and obtaining results that appear worse than they actually are.

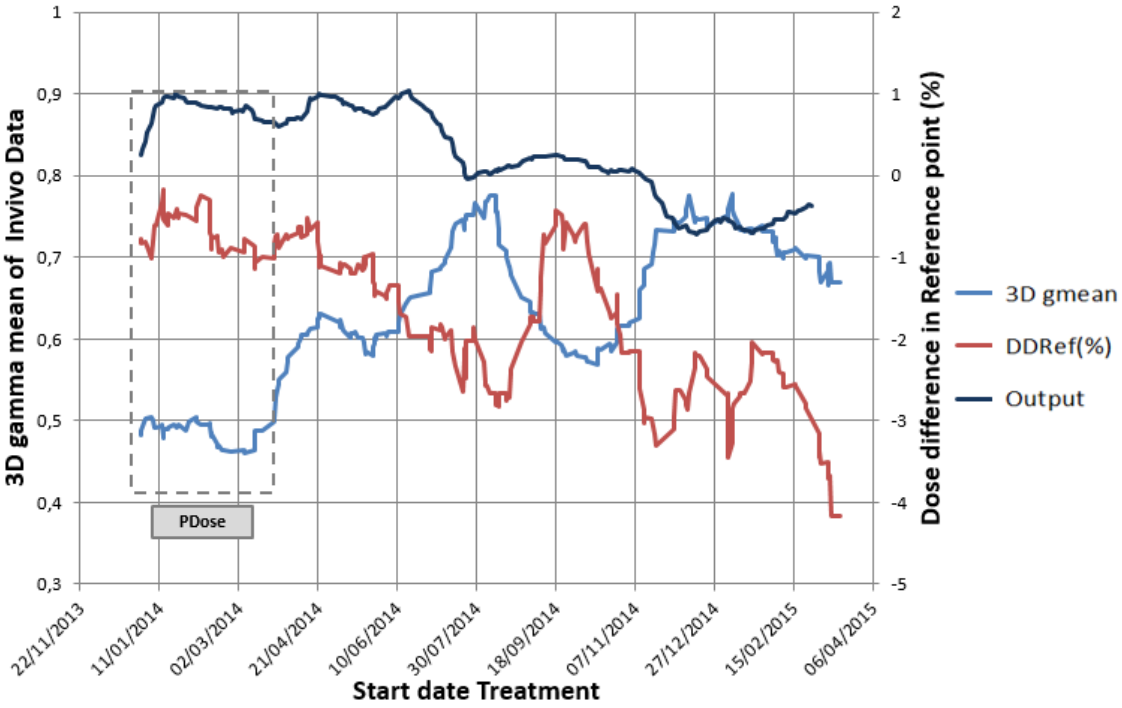

Figure 4.5: Time Trend: EPID *in vivo* measurements for γ_{mean} and Dose difference parameters in PDapp's fraction analysis.

	Dose Ref (%)	**3D** γ_{mean}
Mean	-1.5	0.61
SD	1.8	0.13
Min	-5.8	0.3
Max	3.4	1.06
Sampling: 193		

Table 4.1: Descriptive statistics of the sampling used to perform the time analysis for the parameters Dose Reference Difference and for 3D γ_{mean}.

In relation to the D_{ref} parameter, we observed a systematic underdose over the time trend and it is intensified when the frequency of interlocks occurrence increases or when LINAC output decreases, as seen previously. The causes of this systematic error will be studied in more detail in the next chapter.

4.1.4 DRR Method

We re-calculated 77 patients, using the PDapp DRR option. The comparison between dose estimation with open fields and without (DRR method) are displayed in Figure 4.6 and Figure 4.7 in terms of γ_{mean} and D_{ref} respectively.

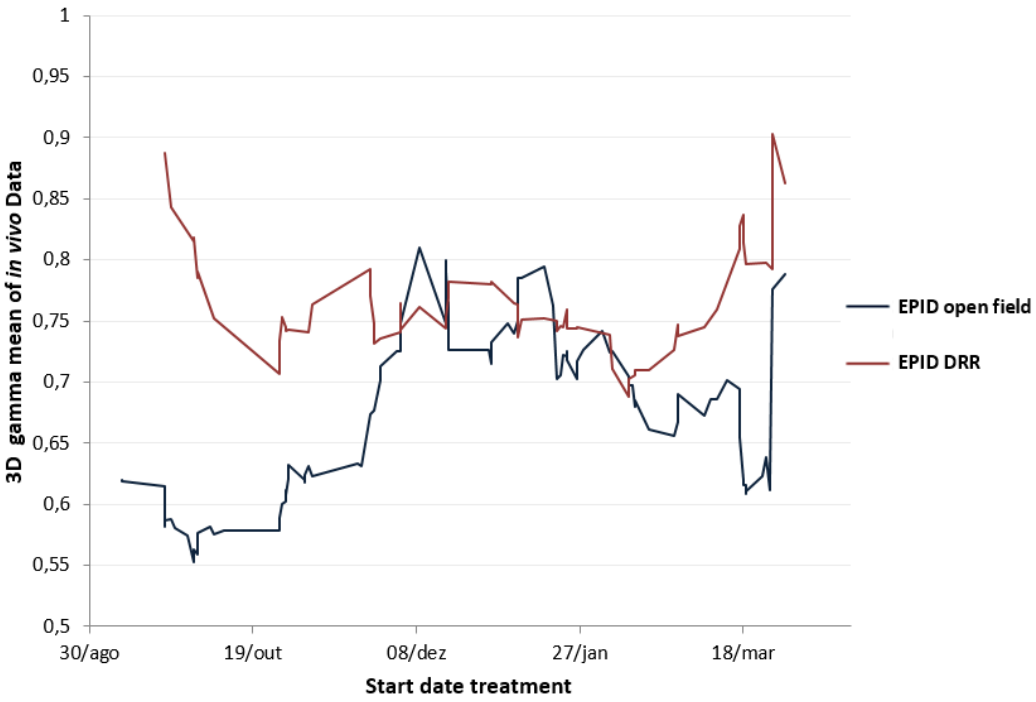

Figure 4.6: Relationship between 3D γ_{mean} over the time for EPID open fields and for EPID DRR methods.

According to Figure 4.6, there is no apparent relationship between these two methods for the γ_{mean} parameter. The only difference between them is the way to obtain the transmission. While the transmission for the DRR method is estimated, the transmission for the open fields method is measured, which suggests that the last method is more accurate. Thus, we expect worse results for the DRR method, which actually happens with the exception of early December and January at the end (the γ_{mean} parameter has higher values).

In relation to the D_{ref} parameter (Figure 4.7), the EPID and DRR curves have similar shapes but the DRR curve is shifted in a vertical direction. The DRR results have mainly an overdose, contrarily of what would be expected. Faced with this reality, together with the fact that γ_{mean} is worse for DRR but better with

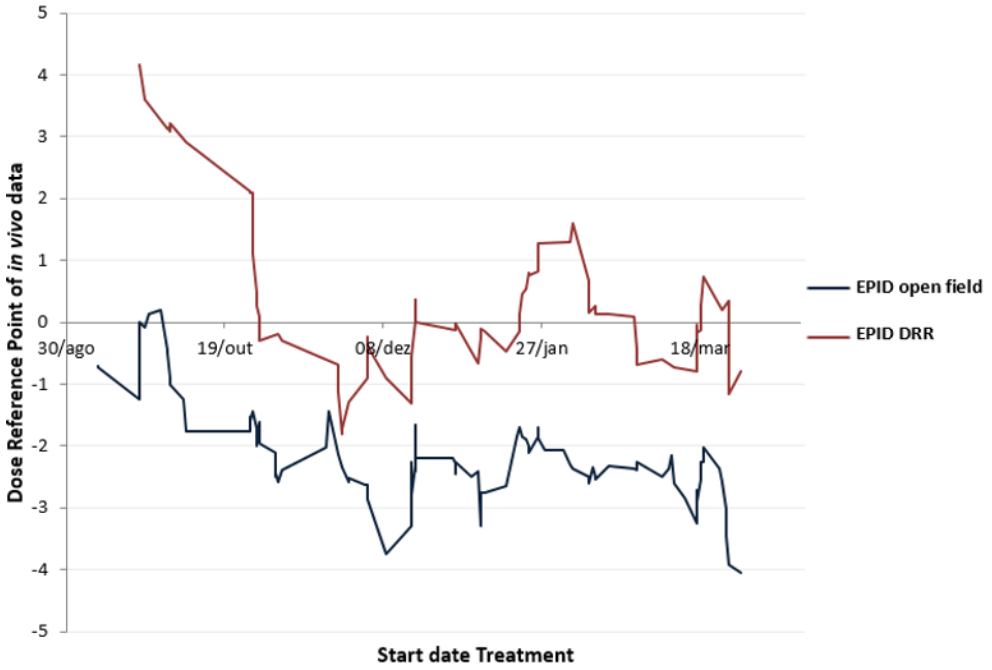

Figure 4.7: Relationship between Dose Reference Point (D_{ref}) parameter over the time for the EPID open fields and EPID DRR method.

respect to the D_{ref} parameter, since dose difference at the isocentre is closer to zero, we are dealing with contradictory data. It is possible to conclude that the DRR method is an inaccurate method that should not be clinically used as a means of dose verification. This inconsistency in terms of results may be related to the new version of PDapp used.

The initial goal was to replace the pre-treatment QA for EPID *in vivo* dosimetry. However, this issue was discussed with the radiotherapy department and it was decided to maintain the pre-treatment QA and, additionally, implement EPID *in vivo* QA. Since resources are insufficient to do both ArcCHECK and EPID measurements, we now intend to perform pre-treatment QA with EPID. This solution is under study but open fields can be used to estimate the dose that is going to be given to the patient. Taking this into account, the advantage present in transmission calculation would no longer be meaningful.

4.1.5 Error Sources

Before clinical implementation of EPID *in vivo* dosimetry, it is important to study some error sources in order to make a correct analysis of the results.

- **Systematic under-dose**

  Gross errors are rare and should be detected during the pre-treatment QA. However, there are many sources of small errors that constantly occur during treatment time. The errors are divided into two groups: the systematic and the random errors. Systematic errors occur if the mean irradiation volume in fractionated treatment (measured dose) differs from the geometry in the treatment plan, more specifically the underdose present in all patients. The fraction-to-fraction variations depending on patient behaviour, in which respiration motion and patient movement are included, are considered random errors.

  The systematic errors are present in all fractions and influence the treatment in the same way. However, the random errors act differently, which could deviate the location of the higher dose in different directions. For that reason the random errors are considered as the changing component of the total error [52].

  – **Prone Cases**

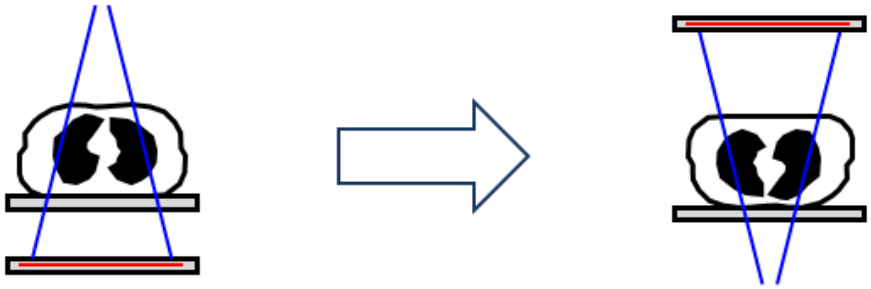

Figure 4.8: Representation of downward beams for a supine position treatment and upward beams for prone position treatments.

The supine position is defined as the position of lying with the face up, as opposed to the prone position, which is with face down. In the supine cases, most beams are directed downward and before they reach the EPID they are absorbed by the couch. For that reason, PDapp applies a couch correction of 3.2% for 6 MV and 2% for 10 MV (Equation 3.11). Note that oblique beams

have greater absorption.

In relation to prone cases, as is seen in Figure 4.8, in most of the fields the radiation transverses first the couch and then the patient. The TPS does not take into account the table, as a consequence, the patient receives effectively less radiation than what actually is prescribed. Since prone patients have upward directed beams (first traversing the couch), these are the worst EPID *in vivo* results.

- **EPID Calibration**

  The calibration itself can be a source of errors, if something went wrong during the acquisition of the EPID images. These images will subsequently be used as a reference and consequently, they will influence all patient results. Table 4.2 shows a case of enormous differences between consecutive images of the same field.

Field Size	$< pixval >$	**#frames**	**Dose**	**Difference**
S_{ij} 26×26	28093	35	9.83E+05	17%
	31955	26	8.31E+05	
20×20	15990	59	9.43E+05	0%
	16264	58	9.43E+05	
5×5	12108	57	6.9E+05	2%
	11939	59	7.04E+05	
10×10	13561	57	7.73 E+05	8%
	13491	62	8.36E+05	

Table 4.2: Pixel values comparison of the acquired images to evaluate the accuracy of the EPID calibration February 2015 for 10 MV.

Relative to sensitivity matrix (S_{ij}) images, we observed a difference of 17%. As mentioned above, this image does not affect the dose at the isocentre, so using the wrong S_{ij} does not explain the poor results associated with the EPID calibration. The differences obtained between two images with 5×5 and 10×10 field sizes were 2% and 8% respectivelly. There is no apparent reason for different EPID dose measures for the same fields. On the other hand, with more complex cases

associated with a higher doses, these differences were not observed. In 14 consecutive measurements of one patient field, only one case differs by 6% from the others.

These differences could be associated with the waiting time required to acquire a dark image between the acquisition of two consecutive images. The dark image is essential to eliminate the bias voltage that can vary during the time. If the bias voltage has a variation and the *Iview* System did not have time to acquire new dark images, these differences will be present in all acquired images. The final image is the average of all the frames multiplied by the number of frames acquired. So a small difference present in each frame becomes bigger after their combination. As a consequence, fields with low dose are more sensitive to bias voltage variations than those having a higher dose. This may be an explanation, since this situation does not occur in patient cases (associated with a higher dose). However, this instability is still unexplained.

Field Size	γ_{mean}	$\%\gamma < 1$	$D_{isoc}(\%)$
5×5	0.3	100	0.9
	0.22	99.6	0.3
10×10	0.68	86.2	2.9
	0.16	100	0.3
20×20	0.17	99.6	0.5
	0.17	99.6	0.5

Table 4.3: Impact of differences in pixel intensity in gamma evaluation.

Analysing the impact of the pixel value differences in gamma evaluation (Table 4.3), an enormous difference can be seen for the reference field (10×10) when using the correct and the wrong EPID image. For the $\%\gamma < 1$ parameter, the first image achieved 100% while the second one has 86.2%, and a D_{isoc} of 0.3% and 2.9% respectively. Recall that the reference field is the one used to perform the EPID calibration. An error of 8% with an homogeneous field in a slab phantom represents a greater error (around 15%) in $\%\gamma < 1$, if we use this image to evaluate the patients.

- **Interlocks**

In order to study the effect of the interlocks in gamma evaluation results, we acquired new open fields in patients who had open fields with interlock. According to the back-projection algorithm, the software uses the open fields for each fraction, more specifically for each field. For that reason, if one open field is not acquired properly, it will affect the entire dose calculation. Although the highest number of the interlocks occur during the treatment (*in vivo*), these fields are not directly comparable, since in one day the patient's anatomy, movement, and position could be different than in the other fractions (days). For this reason, it was decided to make the comparison between open fields that are acquired in the same way and under the same conditions.

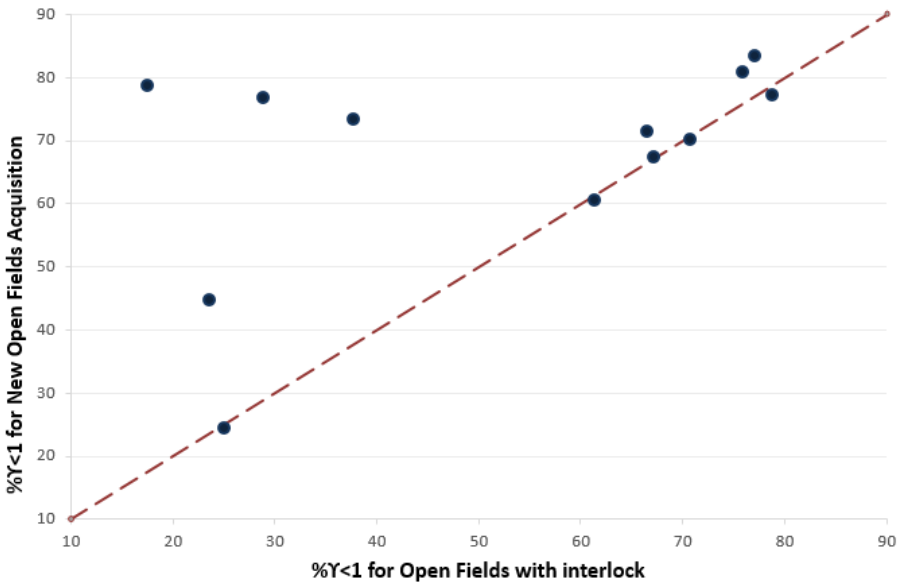

Figure 4.9: Comparison between $\%\gamma < 1$ obtained by using open fields with interlock for PDapp's fraction analysis and after the acquisition of new open fields.

For a sampling of 12 cases, from the dashed line it is possible to see that in 4 of 12 cases the open fields without interlock present much better results than open fields with interlocks. It is also important to note that the largest observed differences occur when there is more than one field with interlock and when the interlock consequences are more severe.

It is easy to see that the $\%\gamma < 1$ decreases as the number of the interlocks increases (Figure 4.10). This information leads us to conclude that the interlocks really affect the EPID results, negatively. The reason for this to happen may be related with three independent sources of error. It could be that the *Iview* does

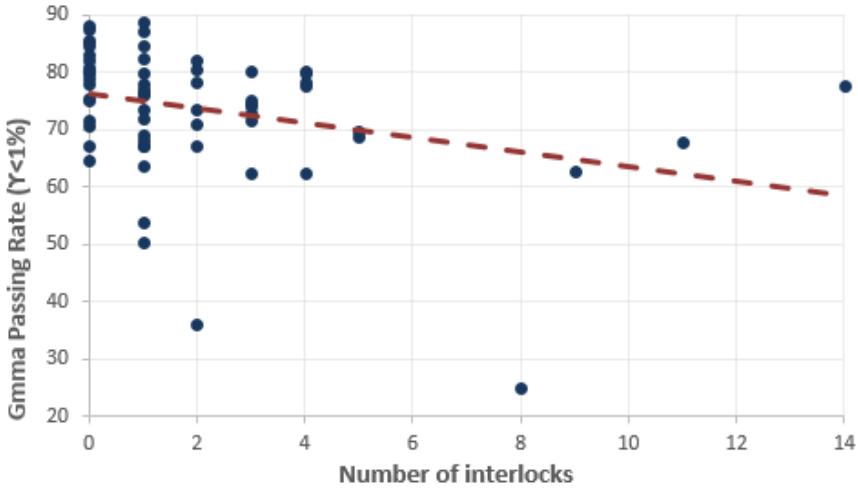

Figure 4.10: Relationship between the gamma passing rate ($\%\gamma < 1$) parameter and the number of interlocks in fraction analysis.

not acquire the remaining image, or that the PDapp does not properly account the total number of images to the field in question, or, and this is a worst case, the LINAC truly delivers less dose.

Figure 4.11 shows a severe case of interlock error. This image surely suggests that the interlock is associated with a measured underdose since the EPID image with interlock (right) has dose only in one side. Therefore, this error must be taken into account because otherwise it will cause a false-positive result that does not correspond to reality.

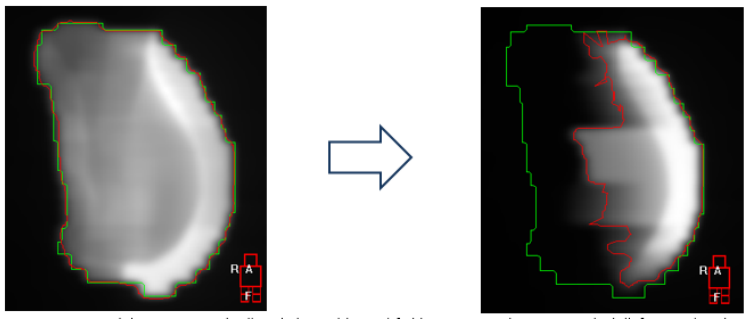

Figure 4.11: Match between EPID (red) and planned (green) field contours without an interlock (left image) and with interlock (on the right).

- **Output Variation**

  It is also interesting to study the effect of the LINAC's output variations on EPID results. The varation was simulated and its impact was evaluated for two different patients in terms of γ_{mean} and $\%\gamma < 1$ parameters (Figures 4.12 and 4.13).

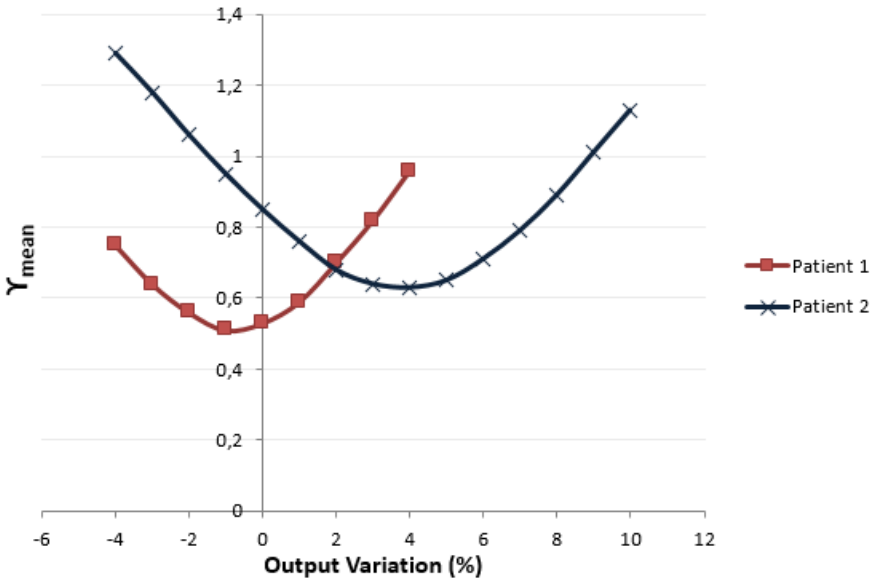

Figure 4.12: Output variation as a function of the γ_{mean} parameter for two different patients.

Two patients with different results (with no output variation) were purposely chosen: patient 1 with 90% of $\%\gamma < 1$ and patient 2 with about 60%. Focusing on patient 1 for both parameters (Figure 4.13 and 4.12), it is noted that the results grow worse as the output varies. On the other hand, for patient 2 if the output increases the results become better. For example, if we increase the output by 1%, the $\%\gamma < 1$ increases 10%. In contrast, a decrease of LINAC output worsens the results, since it decreases $\%\gamma < 1$ and consequently increases the γ_{mean}.

After analysing these graphics, one can conclude that it is extremely important to know if there are large changes in the LINAC output, because it will severely influence the EPID results. On the one hand, a treatment that was given in an accurate way (patient 1) could be considered a poor treatment delivery. On the other hand, a treatment that actually had some errors, could be well evaluated if the LINAC output increases (positive-false case). Besides the EPID results, it is

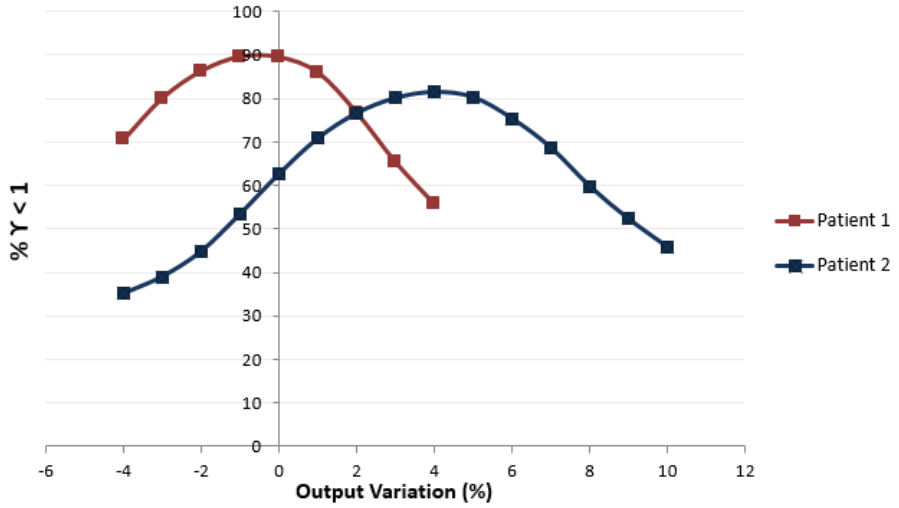

Figure 4.13: LINAC output variation as a function of the $\%\gamma < 1$ parameter for two different patients.

important to mention that LINAC output variations are true errors, which means that patients are truly underdosed or overdosed.

4.1.6 Current Gamma Thresholds

Currently the ArcCHECK pre-treatment QA has a threshold of 90% for $\%\gamma < 1$, and below this value the plans are rejected. In order to implement the EPID *in vivo* dosimetry, it is crucial to define threshold values for the gamma evaluation parameters. These values were obtained based on the sample of 197 patients evaluated.

	First Fraction			**Best of 3 Fractions**		
	γ_{mean}	$\gamma < 1\%$	D_{ref}	γ_{mean}	$\gamma < 1\%$	$D_{ref}(\%)$
Mean	0.64	0.81	-1.54	0.61	0.83	-1.17
SD	0.12	0.09	2.24	0.11	0.08	1.90
Tresh: mean ± 2SD	0.88	0.63	-6 to 3	0.82	0.68	-5 to 3

Table 4.4: Threshold values for the SD method.

Table 4.4 reports the estimated threshold values for the EPID *in vivo* measurements for SD method. The threshold values using the first fraction or the best of

three fractions are very similar as in comparison with the Quartile method. Focusing on first fraction results for the γ_{mean} parameter, treatments that have values above 0.88 are rejected. Before concluding that the internal anatomy or patient's movement was the cause it is important to eliminate that possibility that we have prone patient case, are using the wrong calibration, or if an interlock occured during the irradiation. If none of these are the case, it is advisable to re-plan the treatment in order to balance the maximum and minimum doses according to the magnitude of the measured error. The same procedure should be followed when $\%\gamma < 1$ is below 63% and D_{ref} out of the range -6 to 3 cGy.

4.1.7 EPID dosimetry vs ArcCHECK

Today, in this institution the pre-treatment QA is done only with the ArcCHECK. In addition to the evaluation of *in vivo* results it was important to compare these results with a reliable device. Therefore, the 197 patient measured *in vivo* were then compared with respective pre-treatment results measured by ArcCHECK (Figure 4.14).

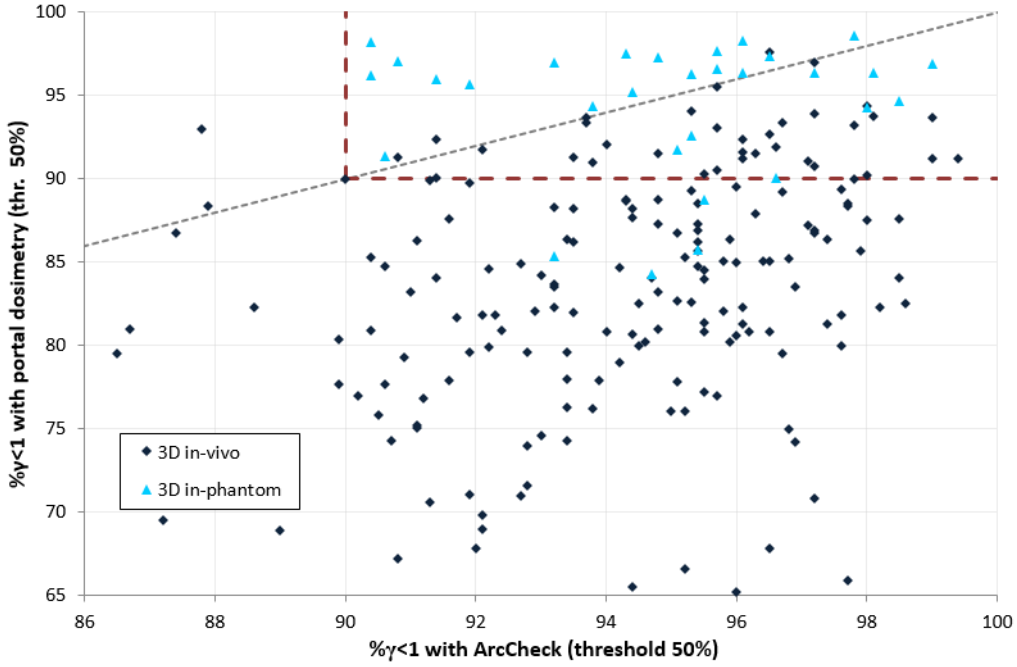

Figure 4.14: Comparison between the ArcCHECK QA results, EPID *in vivo* results (blue) and EPID measurements on ArcCHECK phantom.

The red dashed line represents the actual threshold for $\gamma < 1\%$, 90% in this

case, for the ArcCHECK. As expected, the ArcCHECK pre-treatment results are much better than the EPID *in vivo*. Examining the results, only five EPID *in vivo* measurements are better than the corresponding ArcCHECK evaluations.

In order to close the gap between these two systems and make the results more comparable, we measured the patient plan in a phantom (ArcCHECK) with the EPID in order to simulate the pre-treatment situation. Here, the situation is reversed and only five patients are better with ArcCHECK than with EPID. However, these results are not directly comparable since they are different systems with different sensitivities and there are many of errors that inevitably occur during the patient treatment, which does not happen in a phantom. For that reason, it was also interesting to compare the dose measured by the EPID in a phantom.

4.2 EPID Pre-treatment QA

EPID pre-treatment preliminary QA results were obtained by comparing the calculated and measured dose through gamma evaluation. They are described in the following tables (Tables 4.5 and 4.6) relating to IMRT and VMAT plans respectively.

Despite all the made approaches, as the comparison of the dose at different distances from the head LINAC, the results obtained were better than expected. Different distances involve different head scatter contributions, which influence the results.

Analysing the results for the IMRT plans (Table 4.5) we see that all patients present a mean of $\%\gamma < 1$ higher than 90% and a mean dose difference at a reference point less than 1 or -1%. However, there are three patients that have one field with $\gamma < 1\%$ less than 90% and 2 patients with 2 fields in this situation - analogous to the γ_{mean} and D_{ref} parameters, which present a higher value and a larger difference respectively in these specific cases.

However, and taking into account that in most cases good results are obtained and the worst results have no predominance in any specific field, there is no logical reason for this to happen. It is crucial to measure the patients with the poorest results again with and without a phantom, in order to check if better results are obtained. If the results remain the same, it may suggest that probably the treatment plan was too complex and the LINAC was not able to deliver 100% of the planned dose.

IMRT plans										
		Mean			Max			Min		
Patient	**# Fields**	γ_{mean}	$\gamma < 1\%$	$D_{max}(\%)$	γ_{mean}	$\gamma < 1\%$	$D_{max}(\%)$	γ_{mean}	$\gamma < 1\%$	$D_{max}(\%)$
1	7	0.49	94.10	0.26	0.26	98.82	1.42	0.41	83.24	-2.56
2	6	0.49	94.56	-0.91	0.64	99.05	0.64	0.38	83.41	-2.32
3	5	0.44	95.87	-0.89	0.61	99.38	1.59	0.34	85.08	-7.37
4	6	0.41	97.27	-0.17	0.53	99.93	1.37	0.35	90.55	-2.22
5	7	0.50	94.57	0.26	0.64	99.46	2.33	0.41	85.96	-3.86
6	7	0.43	95.88	0.27	0.47	98.38	3.88	0.40	93.62	-3.78
7	7	0.48	95.98	-0.06	0.55	99.32	0.82	0.39	91.49	-1.88
8	8	0.51	93.63	-0.43	0.68	97.83	2.29	0.40	85.29	-2.27
9	5	0.51	94.39	-1-10	0.58	97.98	1.49	0.44	90.97	-2.95
10	6	0.46	97.22	0.54	0.48	98.61	1.80	0.43	95.37	-0.69
	Mean	0.47	95.35	-0.22	0.58	98.88	1.76	0.4	88.50	-2.99
	SD	0.04	1.28	0.58	0.07	0.68	0.92	0.03	4.41	1.79

Table 4.5: EPID pre-treatment QA results for 10 IMRT plans.

Figure 4.15 shows a successful EPID pre-treatment QA case, since it has 98% of $\%\gamma < 1$, 0.45 of γ_{mean} and a D_{ref} of only 1.19% (Table 4.5). The results obtained are in agreement with what is observed in the images, as the contours represented by different colours (corresponding to different doses), are similar. The planned image is a bit blurred, which can be explained by the degree of precision (3%) with which it was calculated. In relation to gamma evaluation, the white colour represents the situations in which gamma is zero, where the dose difference and DTA agree in 100%, the green and yellow represent a slight difference above and below the planned dose respectively.

Besides the parameter results, it can be seen that for both axes (x and y) the planned and measured profile has the same shape and similar dose magnitude.

For VMAT plans (Table 4.6), only four patients (1, 2, 3, and 4) present $\%\gamma < 1$ higher than 90%. We can also se a systematically underdose (D_{ref} parameter) with a magnitude much larger than the one observed in IMRT plans. The difference between IMRT and VMAT results can be associated with two independent facts. The first is related with the comparison between the entire treatment (VMAT plans) with a dose delivery around 144cGy and one field in IMRT plans, which represents a small part of the treatment with a dose delivered of about 30cGy. A poorer result

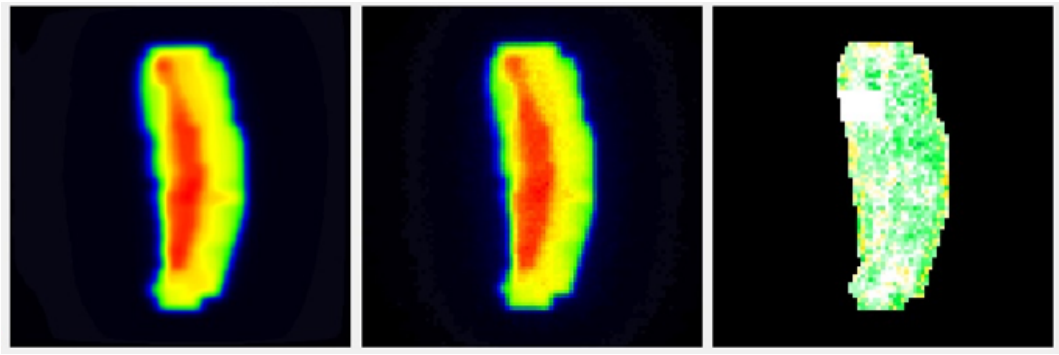

Figure 4.15: Measured (left) and Planned (centre) dose of patient 10 (IMRT plans – Table 4.5), field OAD2 displayed on a colour scale, blue represents the lowest dose and red the highest. The comparison between these two images is done through gamma evaluation (right).

VMAT plans				
Patient	γ_{mean}	$\%\gamma < 1$	$D_{max}(\%)$	**Planned Dose (cGy)**
1	0.34	96.22	-3.65	155.95
2	0.47	97.21	-1.25	138.41
3	0.52	95.62	-2.43	151.99
4	0.55	94.83	-3.38	138.01
5	0.66	82	-1.75	149.87
6	0.59	89.02	-2.93	159.09
7	0.68	84.49	-1.44	129.94
8	0.64	82.6	-4.38	152.48
9	0.64	84.68	-1.36	138.19
Mean	0.57	89,63	-2.51	
SD	0.11	6.35	1.14	

Table 4.6: EPID pre-treatment QA results for 9 VMAT plans.

in one IMRT field can be neglected if all the other fields pass the defined criterion since the overall result will remain good. The other source of error can be related with PDapp Software that was initially developed to calculate the dose inside patient/phantom only for IMRT plans.

Another important fact that is presented in all VMAT and some IMRT cases that could influence the results is the EPID failure in one specific area. It occurred

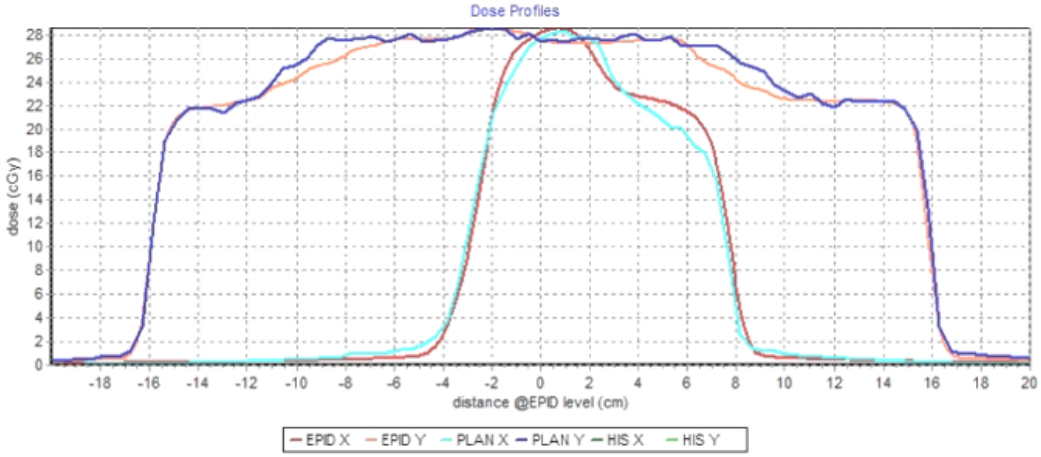

Figure 4.16: Dose Profiles for patient 10, field OAD2 along the reference point plane for planned dose (light blue and dark blue) and measured dose (red and orange according to the x and y planes respectively).

between June/July 2015 until now and the VMAT measurements were performed after that. The software does not account for this area to evaluate, which once again is an approximation of the results.

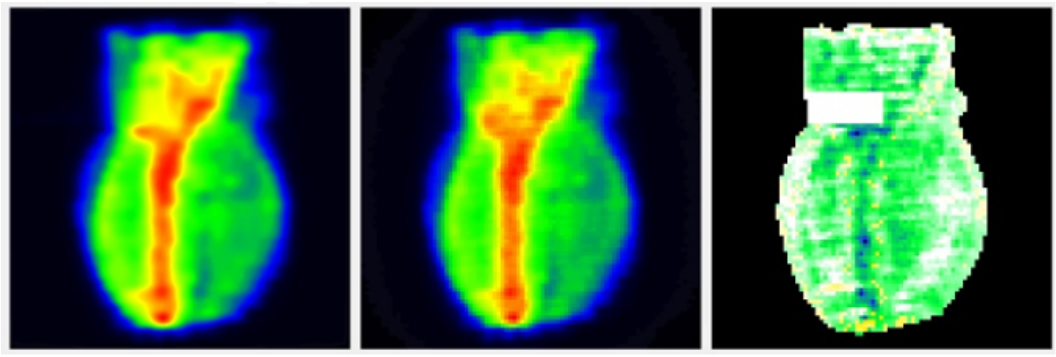

Figure 4.17: Measured (left) and Planned (centre) dose of patient 9 (VMAT plans – Table 4.6) displayed on a colour scale, blue represents the lowest dose and red the highest. The comparison between these two images is done through gamma evaluation (right).

As seen in Figure 4.17, it is possible to see the EPID block that no longer works.

Despite all the approaches mentioned and even though some results remain unexplained, we obtained very encouraging results for both types of plan, which en-

courages the continuation of the study for the future implementation of the EPID pre-treatment QA. The big advantage associated with this change is the EPID high level of precision and sensitivity when compared to that of ArcCHECK. The other advantage is reducing time QA and greater ease to EPID use since it is only required to make an open fields measurements which will subsequently be used for *in vivo*. Contrary to *in vivo* measurements, with EPID pre-treatment QA it is possible to evaluate not only the IMRT plans, but also the VMAT plans whose fields fit in the EPID area.

In the near future and in order to optimize the EPID pre-treatment QA, it is important to calculate the dose directly from each EPID image without having to resort the PDapp software. To convert pixel to dose one must have the IC measurement, in order to have the dose at the isocentre. The sensitivity matrix distinguishes each pixel response and correlates with the isocentre pixel. Besides these steps, it is required to remove the scatter within the EPID, which, thanks to the global calibration model, is already calculated without the need to proceed to additional measurements. This EPID pre-treatment QA version will become easier and much faster to execute. Then, and in order to check if the PDapp was a source of error for VMAT plans, the same analysis could be performed for the poorest cases.

On the other hand, it would be interesting to re-calculate the patient's plans in a phantom with around $7 electrons/cm^3$ of electron density for copper ($9 g/cm^3$ of density) in Monaco. This procedure would seek to replicate as nearly as possible the situation that occurs in the EPID with 3mm copper layer. This step not only eliminates completely the scatter radiation from the patient, it also allows that the maximum dose achieved in the build-up region reaches its maximum at a lower depth. Therefore, it is necessary to re-calculate the plans with a higher degree of precision because the maximum dose peak is reached at a lower depth.

4.3 RTP plans

The parameters investigated that were obtained from the RTP files were the number of CP, number of MU, number of fields and segments, mean segment area, and number of opposing leaves that have a distance less than 0.5 cm. We found no relationship between the ArcCHECK QA measurements and these parameters, as reported in Figure 4.18 for number of CP and MU.

On the other hand, for the EPID results a correlation was found for the number of CP, MU, fields, and segments (Figures 4.21 and 4.22). It was also interesting

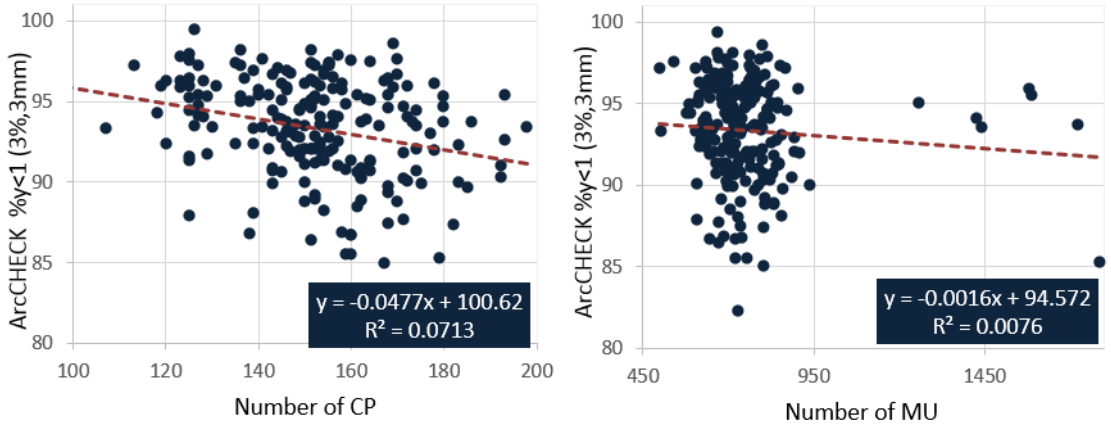

Figure 4.18: Gamma passing rate ($\%\gamma < 1$) parameter measured with ArcCHECK as a function of total number of CP (left) and MU (right) for 202 IMRT breast plans.

to compare the ArcCHECK results for the same 23 IMRT breast cancer patients measured with EPID (Figures 4.19 and 4.20).

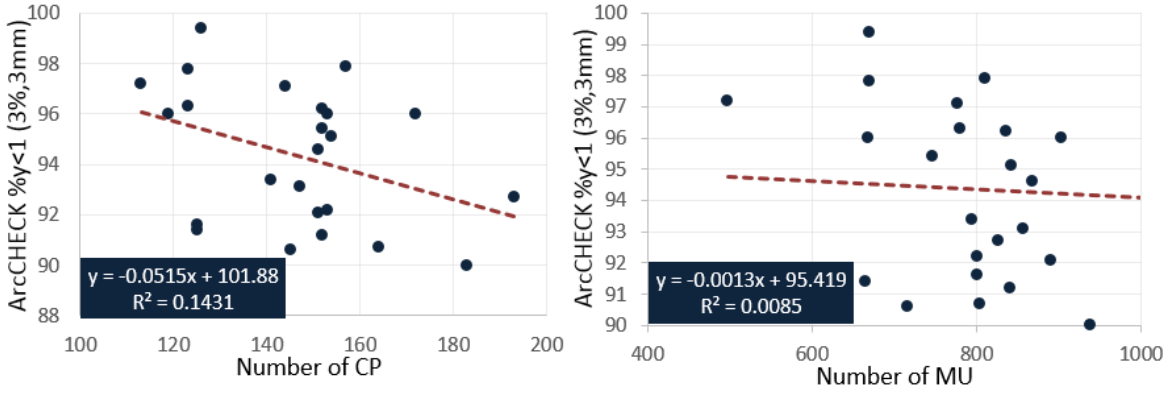

Figure 4.19: Gamma passing rate ($\%\gamma < 1$) parameter measured with ArcCHECK as a function of total number of CP (left) and MU (right) for 23 IMRT breast plans.

In relation to these ArcCHECK results for the 23 patients evaluated by EPID, only the total number of fields (Figure 4.20 on the left side) reveals a small relationship with an adjusted R^2 of 0.21. Although the $\%\gamma < 1$ parameter decreases as the number of fields increases, the results show a wide variety, which precludes choosing a number of fields from which plans should not be produced.

With the exception of the mean field area parameter, all parameters have a statistically significant correlation (Figure 4.21 and 4.22). The adjusted R^2 associated

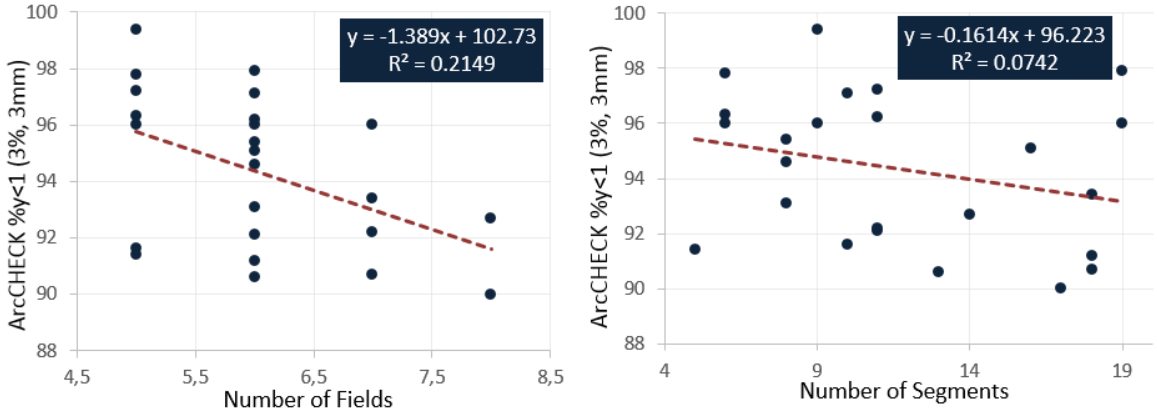

Figure 4.20: Gamma passing rate ($\%\gamma < 1$) parameter measured with ArcCHECK as a function of total number of Fields (left) and Segments (right) for 23 IMRT breast plans.

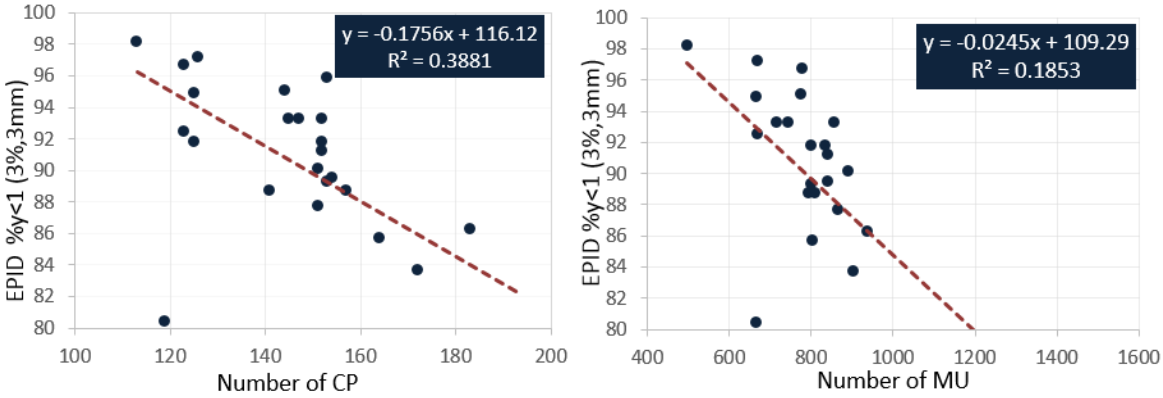

Figure 4.21: Gamma passing rate ($\%\gamma < 1$) parameter measured with EPID as a function of total number of CP (left) and MU (right) for 23 IMRT breast plans.

with number of CP measured by AC (Figure 21 – left) is 0.14 and when measured by EPID is 0.39 (Figure 4.21 – left). Regarding the total number of fields, for AC measurements we obtained a adjusted R^2 of 0.21 (Figure 4.20 – left) instead of 0.4 with EPID (Figure 4.22 – left). As observed with the EPID device, the correlations obtained were much more accurate, as reflected in a greater degree of accuracy compared to ArcCHECK.

Making an interpretative analysis of the correlations obtained it is possible to deduce that a more complex treatment usually takes longer, which is associated with the greater contribution received from the leaf, interleaf and leaf end transmission, and scatter. Therefore, it was expected that the high number of CP, fields, and segments were associated with a poor QA since they are considered a complex

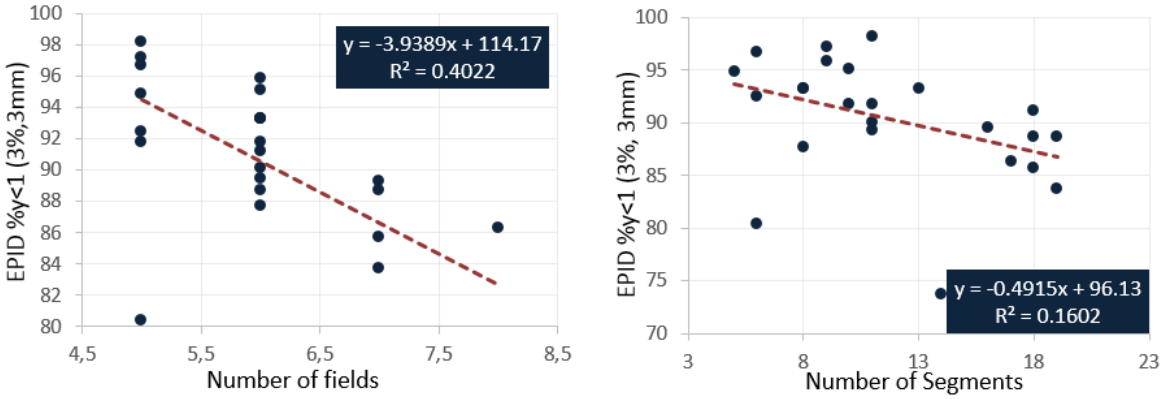

Figure 4.22: Gamma passing rate ($\%\gamma < 1$) parameter measured with EPID as a function of total number of fields (left) and segments (right) for 23 IMRT breast plans.

treatment. A longer treatment also requires more MU to deliver and an increased number of fields. Besides the scatter factors, also the MONACO and LINAC accuracy are also expected to decrease with modulation and small fields. Therefore, it was expected that the QA results would worsen as the MU and number of fields increases. Unlike the ArcCHECK results, the EPID results confirmed what was expected (Figure 4.21 and 4.22).

The LINAC's output depends on head scatter, phantom scatter and backscatter from the collimator jaws and MLC into the monitor chambers. Among other things, these factors are extremely influenced by the field size. A smaller field size decreases the phantom scatter and the scattered radiation from the LINAC head. On the other hand, it increases the backscatter radiation since the MLC and jaws are almost closed. As a consequence, this leads to a smaller dose delivery for the same amount of applied MU. Therefore, it was expected that the small fields, and also the big fields would influence the QA results. However, we found no correlation between the mean field area, SAS<0.5 cm, and the number of fields that have an area less than 0.5 cm as a function of $\%\gamma < 1$.

We expected that for a specific open criteria, as the SAS value increases the QA value would decrease, but no relationship was found.

The MCS parameter defines the complexity of the total treatment plan. It is therefore expected that as the treatment plan becomes more complex, the QA results would become worse.

Figure 4.23 illustrates the relationship between MCS and QA results and as can

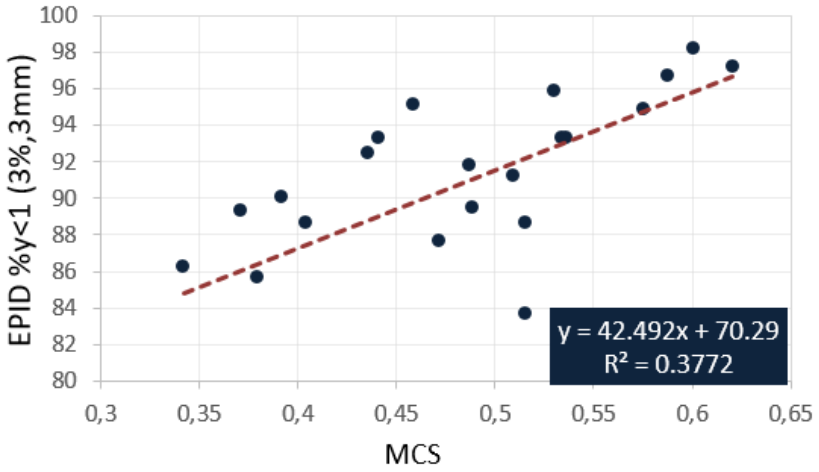

Figure 4.23: Gamma passing rate ($\%\gamma < 1$) parameter as a function of Modulation Complexity Score (MCS) for 22 IMRT breast plans.

be seen, there is a correlation between them with adjusted R^2 of 0.38. This figure also suggests that the $\%\gamma < 1$ parameter increases as MCS increases (the plan becomes simpler). It is important to mention that a MCS of one defines an open rectangular beam with uniform dose distribution. This indication thus supports the expectations that the more complex the beam is, the greater the possibility that the absorbed dose differs from the desired one. However, and although the results are encouraging, it is critical to have a larger sample in order to obtain a statistically significant correlation.

As a conclusion, despite the good correlations obtained for the total number of CP, fields, and MCS, which could indicate a poor QA, it is not yet possible to define a criterion which will exclude plans from further execution.

Chapter 5

Conclusion

The daily pre-treatment QA enables the detection of specific errors that otherwise would only be detected after the first fraction delivered, with *in vivo* dose verification. In order to make the current procedure easier and more accurate, a software has been developed to replace the ArcCHECK by EPID. In general, very promising results were obtained, which motivates continuation of the software development. The next versions should have an algorithm to automatically calculate the EPID dose from the portal open images, but it would be also very interesting to calculate the patient's plan in a phantom with an electron density similar to copper (7 electrons/cm^3). This would seek to not only reduce the phantom scatter contribution but also increase the maximum absorbed dose, as in the EPID device. Therefore it is expected that, in the near future it will be possible to implement EPID pre-treatment QA in the Elekta LINAC by replacing the current ArcCHECK pre-treatment QA.

The EPID *in vivo* dosimetry is the only method capable of verifying the entire radiotherapy treatment chain. Through PDapp software it is possible to obtain the 3D dose reconstruction inside the patient and compare it with the planned dose by means of gamma evaluation method. There are some factors that inevitably occur during the treatment, such as the anatomic changes between fractions and the patient's movement, which compromise the treatment effectiveness. The EPID sensitivity allows for measuring the error magnitude and concluding, through threshold values defined, about the accuracy of the treatment. However, and taking into account that the breast is a difficult region in which to perform the analysis, due to lung proximity, reliable results were obtained. The sample of 197 patients used in the study of EPID error sources provide findings that encourage clinical implementation the EPID *in vivo* dosimetry in breast cancer patients for Elekta LINAC. As a conclusion, the EPID pre-treatment in combination with EPID *in vivo* dosimetry

is a fast and accurate tool for verification of delivery techniques.

The study of the relationship between the plan parameters and QA results has the intention of preventing the realization of QA plans that should apparently be rejected. The most conclusive results were obtained using the EPID device in which a statistically significant correlation was identified between the number of CP, fields, and MCS and $\%\gamma < 1$. Desppite the small sample used, it can be concluded that the more complex the beam is, the greater the possibility that the delivered dose differs from the desired one. However, this information is not yet sufficient to identify plans to be rejected in pre-treatment QA tests. Further study is required.

Bibliography

[1] Sigamani Ashokkumar, N Arunai Nambi Raj, Sujit Nath Sinha, Girigesh Yadav, Rajesh Thiyagarajan, Kothanda Raman, and Manindra Bhushan Mishra. Comparison of Head Scatter Factor for 6MV and 10MV flattened (FB) and Unflattened (FFF) Photon Beam using indigenously Designed Columnar Mini Phantom. *Journal of Medical Physics*, 2014.

[2] World Health Organization. Cancer, 2015.

[3] World Health Organization. Breast cancer: prevention and control, 2015.

[4] American Cancer Society. Global Cancer Facts & Figures 2nd Edition. Technical report, 2011.

[5] International Atomic Energy Agency. Investigation of an Accidental Exposure of Radiotherapy Patients in Panama: Report of a team of experts. Technical report.

[6] D Ash. Lessons from Epinal. *Clinical oncology (Royal College of Radiologists (Great Britain))*, 19(8):614–5, oct 2007.

[7] Mariana Guerrero, X. Allen Li, Matthew A. Earl, Mehrdad Sarfaraz, and Edward Kiggundu. Simultaneous integrated boost for breast cancer using imrt: A radiobiological and treatment planning study. *International Journal of Radiation Oncology Biology Physics*, 59:1513–1522, 2004.

[8] Hilde Van Parijs, Truus Reynders, Karina Heuninckx, Dirk Verellen, Guy Storme, and Mark De Ridder. Breast conserving treatment for breast cancer: dosimetric comparison of sequential versus simultaneous integrated photon boost. *BioMed research international*, 2014:827475, jan 2014.

[9] George Plataniotis. Hypofractionated radiotherapy in the treatment of early breast cancer. *World journal of radiology*, 2:197–202, 2010.

[10] Roger Dale. Use of the linear-quadratic radiobiological model for quantifying kidney response in targeted radiotherapy. *Cancer biotherapy & radiopharmaceuticals*, 19(3):363–70, 2004.

[11] Jack F Fowler. The radiobiology of prostate cancer including new aspects of fractionated radiotherapy. *Acta oncologica (Stockholm, Sweden)*, 44(3):265–276, 2005.

[12] MC Joiner and A van der Kogel. *Basic Clinical Radiobiology Fourth Edition*. 2009.

[13] Amy Yuen Meei Teh, Lorraine Walsh, Thomas G. Purdie, Allen Mosseri, Wei Xu, Wilfred Levin, C. Anne Koch, Anthony Fyles, Fei Fei Liu, and B. C John Cho. Concomitant intensity modulated boost during whole breast hypofractionated radiotherapy - A feasibility and toxicity study. *Radiotherapy and Oncology*, 102:89–95, 2012.

[14] Simone L Alford, Georgina N Prassas, Cathy R Vogelesang, Heather J Leggett, and Chris S Hamilton. Adjuvant breast radiotherapy using a simultaneous integrated boost: clinical and dosimetric perspectives. *Journal of medical imaging and radiation oncology*, 57(2):222–9, apr 2013.

[15] Kathryn D. Held. *Radiobiology for the Radiologist, 6th ed., by Eric J. Hall and Amato J. Giaccia*, volume 166. 2006.

[16] E. B. Podgorsak and Kristofer Kainz. Radiation Oncology Physics: A Handbook for Teachers and Students. *Medical Physics*, 33(6):1920, 2006.

[17] Faiz M Khan. *The physics of radiation therapy*. Third edition, 2003.

[18] Pierre Scalliet Todd Pawlicki, Peter Dunscombe, Arno J. Mundt. Elekta Multileaf Collimator. In *Quality and Safety in Radiotherapy*, chapter Elekta Mul. 2010.

[19] Maria João Dias Cardoso. Estudo dosimétrico para implementação da técnica radioterapêutica Volumetric Modulated Arc Therapy (VMAT), 2011.

[20] P M Deluca. *ICRU Report 83, Prescribing, Recording and Reporting Photon-Beam Intesity-Modulated Radiation Therapy (IMRT)*, volume 10. Journal of the ICRU, 2010.

[21] Mudasir Ashraf, Nandigam Janardhan, Perumal Bhavani, Radhakrishan Shivakumar, Syed Ibrahim, Balakrishna Sarangnathan Palreddy Reddy. Jagdessan Surrendharen, Ben Johnson, and Rayees Ahmad Dar Bhagavathula Madhuri.

Dosimetric comparison of 3DCRT versus IMRT in whole breast irradiation of early stage breast cancer. *International Journal of Cancer Therapy and Oncology*, 2014.

[22] B Fraass, K Doppke, M Hunt, G Kutcher, G Starkschall, R Stern, and J Van Dyke. American Association of Physicists in Medicine Radiation Therapy Committee Task Group 53: quality assurance for clinical radiotherapy treatment planning. *Medical physics*, 25(10):1773–1829, 1998.

[23] IAEA. IAEA Technical Reports Series No. 430: Commissioning And Quality Assurance Of Computerized Planning Systems For Radiation Treatment Of Cancer. Technical report, 2006.

[24] Maria Law and Brent Liu. DICOM-RT and Its Utilization in Radiation Therapy1. *Radiographics*, 29(3):655–667, 2009.

[25] B Mijnheer, I Olaciregui-Ruiz, R Rozendaal, J-J Sonke, H Spreeuw, R Tielenburg, M Van Herk, R Vijlbrief, and a Mans. 3D EPID-based in vivo dosimetry for IMRT and VMAT. *Journal of Physics: Conference Series*, 444:012011, jun 2013.

[26] Leah N. McDermott, Markus Wendling, Jan Jakob Sonke, Marcel van Herk, and Ben J. Mijnheer. Replacing Pretreatment Verification With In Vivo EPID Dosimetry for Prostate IMRT. *International Journal of Radiation Oncology Biology Physics*, 67:1568–1577, 2007.

[27] Andrea L McNiven, Michael B Sharpe, and Thomas G Purdie. A new metric for assessing IMRT modulation complexity and plan deliverability. *Medical physics*, 37(2):505–515, 2010.

[28] T Kairn, S B Crowe, J Kenny, R T Knight, and J V Trapp. Predicting the likelihood of QA failure using treatment plan accuracy metrics. *Journal of Physics: Conference Series*, 489:012051, 2014.

[29] S. B. Crowe, T. Kairn, J. Kenny, R. T. Knight, B. Hill, C. M. Langton, and J. V. Trapp. Treatment plan complexity metrics for predicting IMRT pretreatment quality assurance results. *Australasian Physical & Engineering Sciences in Medicine*, 37(3):475–482, 2014.

[30] A Mans, M Wendling, L N McDermott, J J Sonke, R Tielenburg, R Vijlbrief, B Mijnheer, M van Herk, and J C Stroom. Catching errors with in vivo EPID dosimetry. *Medical physics*, 37:2638–2644, 2010.

[31] S Heukelom, J H Lanson, G van Tienhoven, and B J Mijnheer. In vivo dosimetry during tangential breast treatment. *Radiotherapy and oncology : journal of the European Society for Therapeutic Radiology and Oncology*, 22:269–279, 1991.

[32] Th Loncol, J. L. Greffe, S. Vynckier, and P. Scalliet. Entrance and exit dose measurements with semiconductors and thermoluminescent dosemeters: A comparison of methods and in vivo results. *Radiotherapy and Oncology*, 41:179–187, 1996.

[33] Fan Chi Su, Chengyu Shi, and Niko Papanikolaou. Clinical application of GAFCHROMIC EBT film for in vivo dose measurements of total body irradiation radiotherapy. *Applied Radiation and Isotopes*, 66:389–394, 2008.

[34] Paolo Scalchi and P. Francescon. Calibration of a MOSFET detection system for 6-MV in vivo dosimetry. *International Journal of Radiation Oncology Biology Physics*, 40:987–993, 1998.

[35] M. Essers, J.H. Lanson, G. Leunens, T. Schnabel, and B.J. Mijnheer. The accuracy of CT-based inhomogeneity corrections and in vivo dosimetry for the treatment of lung cancer. *Radiotherapy and Oncology*, 37(3):199–208, dec 1995.

[36] Ronald Boellaard, Marcel van Herk, Hans Uiterwaal, and Ben Mijnheer. First clinical tests using a liquid-filled electronic portal imaging device and a convolution model for the verification of the midplane dose. *Radiotherapy and Oncology*, 47(3):303–312, jun 1998.

[37] Fang-Fang Yin. Input/output characteristics of a matrix ion-chamber electronic portal imaging device. *Medical Physics*, 21(9):1447, 1994.

[38] B J Heijmen, K L Pasma, M Kroonwijk, V G Althof, J C de Boer, A G Visser, and H Huizenga. Portal dose measurement in radiotherapy using an electronic portal imaging device (EPID). *Physics in medicine and biology*, 40:1943–1955, 1995.

[39] Markus Wendling, Robert J W Louwe, Leah N McDermott, Jan-Jakob Sonke, Marcel van Herk, and Ben J Mijnheer. Accurate two-dimensional IMRT verification using a back-projection EPID dosimetry method. *Medical physics*, 33:259–273, 2006.

[40] L N McDermott, R J W Louwe, J J Sonke, M B van Herk, and B J Mijnheer. Dose-response and ghosting effects of an amorphous silicon electronic portal imaging device. *Medical physics*, 31(2):285–295, 2004.

[41] Eric Wåhlin. *Dosimetric pre-treatment verification with an electronic portal imaging device*. PhD thesis, 2006.

[42] Larry E. Antonuk, John Yorkston, Weidong Huang, Howard Sandler, Jeffrey H. Siewerdsen, and Youcef El-Mohri. Megavoltage imaging with a large-area, flat-panel, amorphous silicon imager. *International Journal of Radiation Oncology Biology Physics*, 36(3):661–672, 1996.

[43] Ekta Jhala. *Investigation of Dosimetric Characteristics and Exploration of Potential Applications of Amorphous Silicon Detector*. PhD thesis, University of Canterbury, 2006.

[44] R J W Louwe, L N McDermott, J J Sonke, R Tielenburg, M Wendling, M B van Herk, and B J Mijnheer. The long-term stability of amorphous silicon flat panel imaging devices for dosimetry purposes. *Medical physics*, 31(11):2989–2995, 2004.

[45] ELEKTA. Corrective Maintenance Manual - IviewGT, 2006.

[46] Markus Wendling, Leah N McDermott, Anton Mans, Jan-Jakob Sonke, Marcel van Herk, and Ben J Mijnheer. A simple backprojection algorithm for 3D in vivo EPID dosimetry of IMRT treatments. *Medical physics*, 36(7):3310–3321, 2009.

[47] Markus Wendling, Leah N. McDermott, Anton Mans, Igor Olaciregui-Ruiz, Raul Pecharroman-Gallego, Jan-Jakob Sonke, Joep Stroom, Marcel van Herk, and Ben J. Mijnheer. In Aqua vivo EPID dosimetry. *Medical Physics*, 39(1):367, 2012.

[48] Jonas Bengtsson Scherman. *Developement and evaluation of methods for comparison of dose distributions in radiother- apy using calculated , synthetic and simulat- ed measured dose distributions .* PhD thesis, 2009.

[49] Daniel A Low and James F Dempsey. Evaluation of the gamma dose distribution comparison method. *Medical physics*, 30(9):2455–2464, 2003.

[50] D A Low, W B Harms, S Mutic, and J A Purdy. A technique for the quantitative evaluation of dose distributions. *Medical physics*, 25(5):656–661, 1998.

[51] Songwon Seo and Ph D Gary M. Marsh. A review and comparison of methods for detecting outliersin univariate data sets. *Department of Biostatistics, Graduate School of Public Health*, MS - Maste:53+7, 2006.

[52] Marcel Van Herk. Errors and Margins in Radiotherapy. *Seminars in Radiation Oncology*, 14(1):52–64, 2004.

[53] W.P.M. Mayles. The Glasgow Incident — a Physicist's Reflections. *Clinical Oncology*, 19(1):4–7, feb 2007.